Dysprosium complexes with a flat pentadentate donor: in the search for single ion magnets

Matilde Fondo,[§,] Julio Corredoira-Vázquez,[§] Ana M. García-Deibe,[§] Silvia Gómez-Coca,[£] Eliseo Ruiz,[£] and Jesús Sanmartín-Matalobos[§]*

[§] Departamento de Química Inorgánica, Facultade de Química, Universidade de Santiago de Compostela, Campus Vida, 15782 Santiago de Compostela, Spain.

[£] Departament de Química Inorgànica i Orgànica, and Institut de Química Teórica i Computacional, Universitat de Barcelona, 08028 Barcelona, Spain

KEYWORDS: pentadentate N_3O_2 donor, Schiff base, dysprosium complex, imine-hemiacetal, single molecular magnet. Multireference calculations

ABSTRACT: The reactivity of dysprosium(III) nitrate towards the reported pentadentate N_3O_2 Schiff base H_2L (2,6-bis(2-hydroxyphenyliminomethyl)pyridine) has been investigated. This reactivity depends to a large extend on the operational pH of the medium and, accordingly, two different complexes, $[Dy(HL)(NO_3)_2]\cdot H_2O$ (**1**·H_2O) and $[Dy(L)(NO_3)(EtOH)(H_2O)]\cdot 2H_2O$ (**2**·$2H_2O$), were isolated. Besides, reaction of H_2L with dysprosium(III) chloride in methanol yields $[Dy(HL')_2)][Dy(L)(Cl_2)]$ (**3**), where H_2L' (6-(2-hydroxyphenyliminomethyl)-2-methoxyhydroxymethyl)pyridine) is an N_2O_2 hemiacetal donor derived from the partial hydrolysis of the H_2L ligand, and subsequent addition of the methanol solvent to the carbonyl group. Single crystal X-ray diffraction studies of **1**·Py·$0.5CH_3OH$·$0.5H_2O$, **2**·$2H_2O$ and **3** show that the Schiff base acts in all cases as a nearly flat pentadentate donor, and that this behavior is independent of the degree of deprotonation of the phenolic oxygen atoms (monodeprotonated or bisdeprotonated). Therefore, **1**·Py·$0.5CH_3OH$·$0.5H_2O$, **2**·$2H_2O$ and **3** constitute the first lanthanoid complexes of H_2L to be crystallographically characterized. Complexes

1·Py·0.5CH_3OH·0.5H_2O and **2**·2H_2O show DyN_3O_6 cores, with distorted geometries closer to spherical tricapped trigonal prism or spherical capped square antiprism for **1**·Py·0.5CH_3OH·0.5H_2O and **2**·2H_2O, respectively. In the case of **3**, the cation $[Dy(HL')_2)]^+$ shows a dysprosium ion in an N_4O_4 triangular dodecahedron environment, while the $[Dy(L)(Cl_2)]^-$ unit shows a $DyN_3O_2Cl_2$ core with distorted pentagonal bipyramidal geometry. Moreover, attempts to dilute **1**·H_2O with yttrium yielded single crystals of $(Et_3NH)[Dy_{0.09}Y_{0.91}(L)(NO_3)_2]$ (**4**), where the Schiff base shows the same pentadentate chelate coordination mode. Studies on the behavior of **1**·H_2O, **2**·2H_2O and **3** as potential single molecular magnets show that **2**·2H_2O and **3** are field-induced SIMs, while **1**·H_2O does not exhibit frequency-dependent peaks of the out of phase susceptibility even in the presence of an external dc magnetic field. Nevertheless, diluted sample **4** is a SIM at zero dc field. Ab initio calculations using CASSCF methods including spin-orbit effects support these results.

INTRODUCTION

Single molecular magnetism has aroused great interest since its origin, with the discovery of the Mn_{12} magnet by Gatteschi et al.[1] The significance of the field has gradually increased as the potential applications of these compounds, such as high density information storage, spintronics, and quantum computing, have been known.[2-4] Among the achievements of the area in the last 20 years, the discovery of the first single ion magnet (SIM) by Ishikawa and col.,[5] or the publication of the electrostatic model for increasing the anisotropy in single ion f-metal complexes by Reinhart and Long,[6] have been giant steps. Accordingly, these discoveries made the field of molecular magnets focus on mononuclear lanthanoid complexes and, in recent years, this area has increasingly centered on isolating dysprosium(III) compounds with axial geometry. In this way, the improvement in the research of molecular magnets has been absolutely amazing during the last four years, with constant increases in the blocking temperatures (T_B) and effective energy barriers (U_{eff}). Thus, the record-breaking T_B from 2011

to 2016 was 14 K, reached by a dinuclear terbium(III) complex.[7] In 2016, an air stable dysprosium(III) complex with a pentagonal bipyramid (pbp) environment is described as a single ion magnet with T_B = 20 K.[8] In the same year, Winpenny et *al*. published a second pbp Dy^{III} complex that reached the highest U_{eff} reported until that date, but that was unstable in air.[9] In 2017, the metallocene $[Dy(Cp^{ttt})_2][B(C_6F_5)_4]$ (Cp^{ttt} = $C_5H_2{}^tBu_3$-1,2,4) overtook all the blocking temperature records, with T_B = 60 K, and U_{eff} = 1837 K.[10] One year later, J. R. Long and col. published some new metallocenes related to $[Dy(Cp^{ttt})_2][B(C_6F_5)_4]$, with empirical formula $[Dy(Cp^{iPr4R})_2][B(C_6F_5)_4]$ (R = H, Me, Et or Pr^i), and they showed that the substituents on the aromatic ring affected the blocking temperature, in such a way that $[Dy(Cp^{iPr4Me})_2][B(C_6F_5)_4]$ presented U_{eff} = 1468 cm^{-1} (2112 K) and blocking temperature of 62 K.[11] At the same time, Layfield et al. published the air unstable metallocene $[(Cp^{iPr5})Dy(Cp^*)][B(C_6F_5)_4]$ (Cp^{iPr5} = pentaisopropylcyclopentadienyl),[12] with U_{eff} = 1541 cm^{-1} (2217 K) and T_B = 80 K. This blocking temperature breaks the glass ceiling of the liquid nitrogen temperature, what supposes a milestone in the field of molecular magnetism, and it has not been surpassed until now.

Consistent with these findings, it seems that the search for SMMs of high blocking temperature should be focused on the organometallic chemistry of dysprosium. Nevertheless, a handicap of the related metallocene compounds is their air sensitivity. Accordingly, the coordination chemistry could be a sound alternative, since coordination compounds are usually more stable in air. In this way, although no dysprosium(III) coordination complexes with linear geometry were previously described, the pentagonal bipyramid geometry could constitute an option to achieve axiality. However, this geometry is not easy to predetermine in lanthanoid metals, and the reported examples with monodentate ligands seem to be the result of serendipity on many occasions. Therefore, although the use of pentadentate flat chelating donors, joined to coordination of auxiliary quite bulk ligands, could lead to predetermine the pbp geometry, only

few examples of this kind of pentadentate donor have been used to prepare lanthanoid complexes. In this way, it is remarkable the use of an azamacrocycle N_5 ligand,[13] the hydrazone H_4daps (Chart I),[14-16] which usually acts as an N_3O_2 donor, and related hydrazones.[17-23] The coordination chemistry of lanthanoids with the well-known H_4daps ligand clearly differs from that of d-block or main group metals, and the expected pentadentate chelating ability is not always achieved.[16] Accordingly, the chemistry of lanthanoid(III) ions with pentadentate quite flat donors is still poorly explored. With these considerations in mind, we decided to investigate the behavior of a previously reported N_3O_2 Schiff base (Scheme 1) towards dysprosium(III). As far as we know, the chemistry of this ligand with lanthanoid metals is hitherto unknown. The results achieved, which include the study of the obtained samples as potential SIMs, are reported herein.

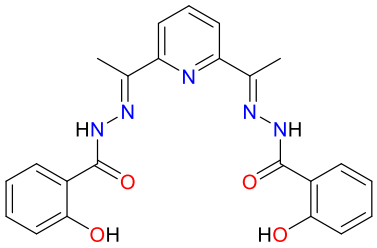

H_4daps

Chart I

EXPERIMENTAL

Materials and general methods. All chemical reagents were purchased from commercial sources, and used as received without further purification. Elemental analyses of C, H and N were performed on a Carlo Erba EA 1108 analyser. Infrared spectra were recorded in the ATR mode on a Varian 670 FT/IR spectrophotometer in the range 4000-500 cm^{-1}. ^1H NMR spectrum of related H_2L was recorded on a Bruker DPX-250 spectrometer. Micro X-ray fluorescence quantitative analyses of Y and Dy for **4** were recorded on a Bruker TORNADO 4 device.

Syntheses of H_2L. H_2L was obtained by a variation of a previously described method,[24] where the ethanol solvent of the reaction is changed by a mixture of chloroform and ethanol, and the ligand was satisfactorily characterized by elemental analysis, IR and ^{1}H NMR spectroscopy. Yield: 97%. Elemental anal. calcd. for $C_{19}H_{15}O_2N_3$ (317): C 71.92, N 13.25, H 4.73 %. Found: C 71.70, N 13.21, H 4.95 %. IR (ATR, $\tilde{\nu}$/cm^{-1}): 1585 (C=N_{py}), 1624 (C=N_{imine}), 3352, 3400 (OH). ^{1}H-RMN (DMSO-d_6, 250 MHz, δ/ppm): 6.94-6.96 (m, 4H), 7.15 (t, 2H), 7.35 (d, 2H), 8.11 (t, 1H), 8.51 (d, 2H), 8.81 (s, 2H), 9.13 (s, 2H).

Syntheses of the complexes. $[Dy(HL)(NO_3)_2]\cdot H_2O$ (**1**·H_2O): A solution of $Dy(NO_3)_3\cdot 6H_2O$ (0.161 g, 0.353 mmol) in ethanol 96% (10 mL) was added to a solution of H_2L (0.112 g, 0.353 mmol) in ethanol 96% (22 mL). The mixture was refluxed for 3 h and the obtained suspension was centrifuged. The mother liquors were decanted and the solid dried in an oven. Yield: 0.111 (51%). Elemental analysis calcd. for $C_{19}H_{16}DyN_5O_9$ (620.50): C 36.74, N 11.28, H 2.58 %. Found: C 36.81, N 11.06, H 2.49 %. IR (ATR, $\tilde{\nu}$/cm^{-1}): 1269, 1475 (NO_3), 1543 (C=N_{py}), 1587 (C=N_{imine}), 3552 (OH).

The same solid is obtained when an ethanolic solution of the ligand is basified with tetramethylammonium hydroxide up to operational pH = 9.4, and then mixed with the dysprosium salt.

Recrystallization of the red solid in pyridine/methanol/toluene by diffusion of diethylether yielded single crystals of $[Dy(HL)(NO_3)_2]\cdot Py\cdot 0.5CH_3OH\cdot 0.5H_2O$ (**1**·$Py\cdot 0.5CH_3OH\cdot 0.5H_2O$), suitable for X-ray diffraction studies.

$[Dy(L)(NO_3)(EtOH)(H_2O)]\cdot 2H_2O$ (**2**·$2H_2O$): To a solution of H_2L (0.094 g, 0.296 mmol) in ethanol 96% (30 mL), $(CH_3CH_2)_3N$ (6 mL, 0.600 mmol) was added. Then, a solution of $Dy(NO_3)_3\cdot 6H_2O$ (0.14 g, 0.307 mmol) in ethanol 96% (10 mL) was incorporated and the mixture refluxed with stirring for 3 h. The resultant solution is filtered to avoid possible impurities, and the filtrate is concentrated up to 20 mL. The obtained suspension was

centrifuged, the mother liquors decanted, and the solid dried in an oven. Yield: 0.049 g (25%). Elemental anal. calcd. for $C_{21}H_{25}DyN_4O_9$ (639.95): C 39.38, N 8.75, H 3.91 %. Found: 39.18, N 8.85, H 4.04 %. IR (ATR, $\tilde{\nu}$/cm^{-1}): 1269, 1455 (NO_3), 1534 ($C{=}N_{py}$), 1585 ($C{=}N_{imine}$), 3230, 3483, 3541 (OH).

Slow evaporation of the mother liquor yielded single crystals suitable for X-ray diffraction studies of **2**·$2H_2O$.

[[Dy(HL')$_2$)][Dy(L)(Cl_2)] (**3**): To a solution of H_2L (0.112 g, 0.353 mmol) in methanol (23 mL) with operational pH = 6.5, a methanolic solution of Me_4NOH 0.5 M was added up to operational pH = 7.2. Then, $DyCl_3·6H_2O$ (0.133 g, 0.353 mmol) was incorporated and the mixture was refluxed with stirring for 3 h. During this time, a red solid is formed, which is collected by filtration, and dried in air. Yield: 0.065 g (30%). Elemental analysis calcd. for $C_{47}H_{39}Dy_2Cl_2N_7O_8$ (1225.75): C 46.01, N 7.99, H 3.18 %. Found: 45.97, N 7.89, H 3.04 %. IR (ATR, $\tilde{\nu}$/cm^{-1}): 1539 ($C{=}N_{py}$), 1583 ($C{=}N_{imine}$), 3327 (OH).

Recrystallization of the crude product in methanol/hexane yielded single crystals suitable for X-ray diffraction studies of **3**.

(Et_3NH)[$Dy_{0.09}Y_{0.91}$(L)(NO_3)$_2$] (**4**): To a solution of H_2L (0.07 g, 0.221 mmol) in ethanol 96% (25 mL), $(CH_3CH_2)_3N$ (4.4 mL, 0.44 mmol) was added. Then, a solution of $Dy(NO_3)_3·6H_2O$ (0.01 g, 0.0219 mmol) and $Y(NO_3)_3·6H_2O$ (0.076 g, 0.198 mmol) in ethanol 96% (10 mL) was incorporated to the basic ligand solution, and the mixture was refluxed with stirring for 3 h. The resultant solution is filtered to avoid possible impurities, and the filtrate is left to slowly evaporate until single crystals of (Et_3NH)[$Dy_{0.09}Y_{0.91}$(L)(NO_3)$_2$], suitable for X-ray diffraction studies, precipitate. Yield: 0.07 g (50%). Elemental analysis calcd. for $C_{25}H_{29}Dy_{0.09}N_6O_8Y_{0.91}$ (637.44): C 47.06, N 13.18, H 4.55 %. Found: C 47.21, N 13.06, H 4.79 %. Micro X- ray fluorescence: % Dy: 9.00; %Y: 91%.

Crystallographic refinement and structure solution. Crystal data and details of refinement are given in Table S1. Single crystals of **1**·Py·0.5CH_3OH·0.5H_2O, **2**·2H_2O, **3** and **4** were obtained as detailed above. Data were collected at 100 K on a Bruker D8 VENTURE PHOTON III-14 diffractometer, employing graphite monochromated Mo-kα (λ = 0.71073 Å) radiation. Multi-scan absorption corrections were applied using SADABS.[25] These structures were solved by standard direct methods, employing SHELXT,[26] and then refined by full matrix least-squares techniques on F^2, using SHELXL from the program package SHELX-2014.[26] All non-hydrogen atoms corresponding to the complexes were refined anisotropically, but in some cases disordered atoms or solvates with low occupation sites were isotropically treated. Hydrogen atoms were typically included in the structure factor calculations in geometrically idealized positions. Non-disordered hydrogen atoms attached to oxygen and/or nitrogen atoms, with partial occupation of 1, were mostly located in the corresponding Fourier maps, with the intention of revealing the hydrogen bonding scheme. In these cases either they were freely refined, or with thermal parameters derived from the parent atoms. When these H atoms could not be located in the Fourier map, they were fixed at reasonable positions.

Powder X-ray diffraction studies. The powder diffractograms for **2**·2H_2O and **3** were recorded on a Philips diffractometer with a control unity type "PW1710", a vertical goniometer type "PW1820/00" and a generator type "Enraf Nonius FR590", operating at 40 kV and 30 mA, using monochromated Cu-Kα (λ = 1.5418 Å) radiation. A scan was performed in the range $2 < 2\theta < 30°$ with t = 3 s and $\Delta 2\theta = 0.02°$. LeBail refinement was obtained with the aid of HighScore Plus Version 3.0d.

Magnetic measurements. Magnetic susceptibility dc and ac measurements for powder crystalline samples of **1**·H_2O, **2**·2H_2O, **3** and **4** were carried out at the Unitat de Mesures Magnètiques of the Universitat de Barcelona with a Quantum Design SQUID MPMS-XL susceptometer. The dc magnetic susceptibility data were recorded under magnetic fields of 190

G (2-30 K) and 3000 G (30-300 K) in the range 2-300 K. Magnetization measurements at 2.0 K were recorded under magnetic fields ranging from 0 to 50000 Oe. Diamagnetic corrections were estimated from Pascal's Tables. Alternating current (ac) susceptibility measurements in different applied static fields (H_{dc} = 0, 1500 or 3000 Oe) were performed with an oscillating ac field of 3.5 Oe and ac frequencies ranging from 4 to 1500 Hz.

Computational Details. CASSCF method was employed to calculate the state energies without spin-orbit effects for mononuclear Dy^{III} complexes while the effect of spin–orbit coupling was taken into account perturbatively in a second step by using the restricted active space state interaction method (RASSI).[27] Dynamic correlation contributions are not essential due to the relatively large ionic character of the Ln-O bonds. The MOLCAS ANO-RCC basis set[28-30] was used for all the atoms. The following contractions were used: Dy [9s8p6d4f3g2h]; Cl [5s4p3d2f]; O [4s3p2d1f]; N [4s3p2d1f]; C [3s2p] and H [2s]. In the CASSCF calculations, a (9,7) active space were used by considering 21 sextets, 128 quadruplets and 98 doublets. The direction and magnitude of the magnetic moment of the final states were evaluated using the SINGLE_ANISO routine implemented in open Molcas.[31] The matrix elements of the transition magnetic moments have been calculated to have an estimation about the probability of transition between two different states of the molecules.[32] Such matrix elements are calculated an integral between the two involved states, as it is proposed by the golden Fermi rule using a magnetic moment operator. DFT calculations were performed to obtain the electrostatic potentials of the ligand environment of the complexes using a model structure in which the metal atom is removed, using the B3LYP[13] functional with a TZVP basis set[14] using the Gaussian 09 package.[15]

RESULTS AND DISCUSSION

Syntheses. The reactivity of H_2L towards $Dy(NO_3)_2 \cdot 6H_2O$ was investigated under different reaction conditions, as shown in Scheme 1.

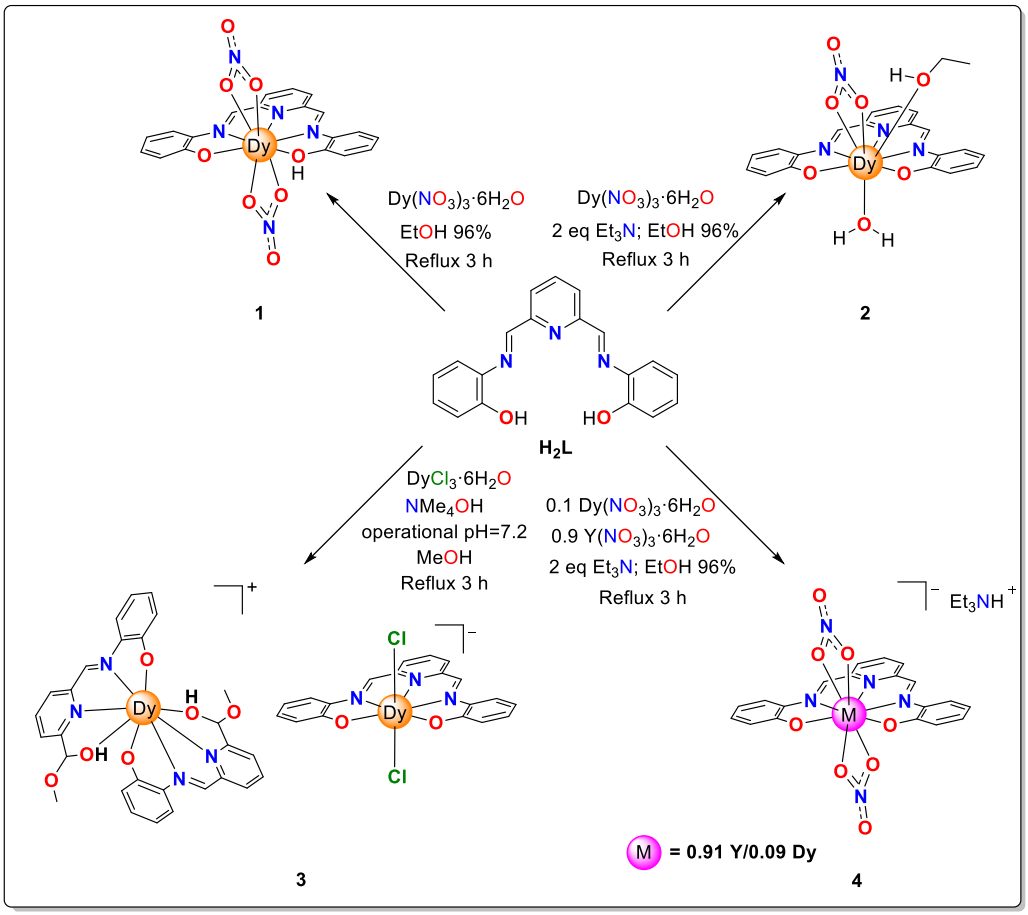

Scheme 1. Reaction scheme for isolation of complexes **1**-**4.**

Thus, when H_2L and $Dy(NO_3)_3 \cdot 6H_2O$ are mixed in 1:1 molar ratio in ethanol 96%, the quite insoluble complex **1**$\cdot H_2O$ precipitates. The same compound is also obtained when an ethanol solution of the ligand, basified with tetramethylammoniun hydroxide up to operational pH = 9.4, is mixed with the dysprosium salt in 1:1 molar ratio. Nevertheless, if an ethanol solution of H_2L is mixed with Et_3N in 1:2 molar ratio, and then $Dy(NO_3)_2 \cdot 6H_2O$ is added in 1:1 (ligand:salt) molar ratio, the very soluble complex **2**$\cdot 2H_2O$ is isolated.

Reaction of $DyCl_3 \cdot 6H_2O$ with a solution of H_2L, basified with tetramethylammoniun hydroxide up to operational pH = 7.2, leads to ionic complex $[Dy(HL')_2)][Dy(L)(Cl_2)]$ (**3**) (Scheme 1). This ionic compound shows that in the $[Dy(HL')_2)]^+$ cation, the dysprosium ion is

surrounded by two $(HL^{\cdot})^{-}$ ligands, which derive from the Schiff base L^{2-} (Scheme 2), and that show a hemiacetal functional group.

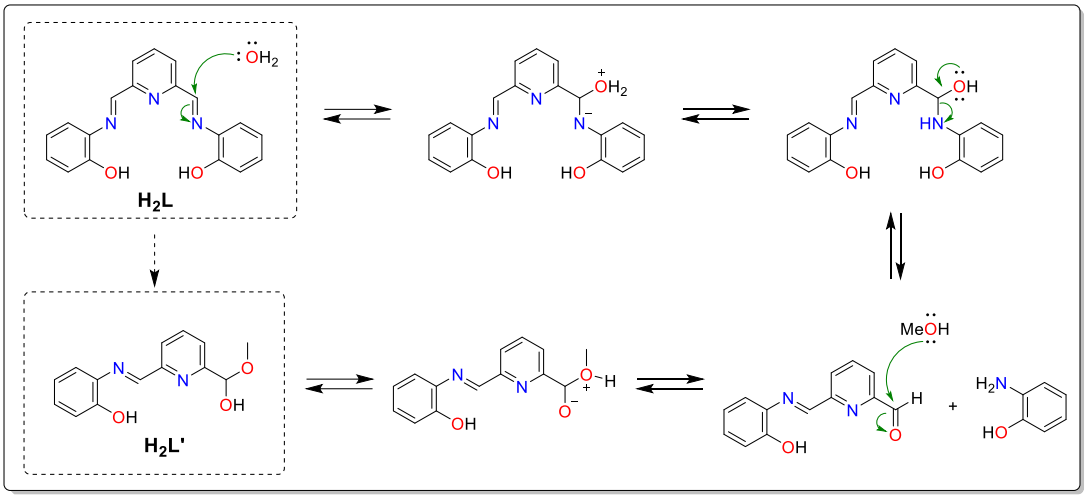

Scheme 2. Proposed mechanism for the formation of hemiacetal from imine functional group

The formation of hemiacetals from aldehydes and alcohols is quite well known, as these are usually developed as intermediates in the preparation of acetals from aldehydes or ketones. Nevertheless, it should be noted that hemiacetals are rather unstable species, and only very small amounts can be obtained if they are not stabilized by structural effects.[33] As far as we know, no many crystallographically characterized complexes containing hemiacetals as ligands has been reported up to now. These scarce examples usually contain d-metals[34-39] but, to the best of our knowledge, no hemiacetal complexes have been described with lanthanoid metal ions. Besides, most of the reported complexes were obtained by conversion of aldehydes, and, as far as we know, only one case was reported where the hemiacetal donor comes from an imine ligand.[37] This conversion of imines into hemiacetals, summarized in Scheme 2, seems to be catalysed by coordination to the metal ion.[37] This can readily be inferred from the fact that the Schiff base H_2L can be obtained in alcohols without any evidence of decomposition in this or related works.[24] Nevertheless, the operational pH of the medium and/or the presence of chloride in the reaction medium must play an important role in the formation of the hemiacetal from solvolysis of the coordinated imine, given that the Schiff base is intact in complexes **1**·H_2O and

2·2H_2O. The efforts made to carry out the same reaction in a non-alcoholic medium, such as acetonitrile or THF, were unfruitful, and the isolated solids could not be satisfactorily characterized.

Moreover, attempts were made to obtain a diluted sample of **1**·H_2O, of stoichiometry [$Dy_{0.09}Y_{0.91}(HL)(NO_3)_2$]. Thus, mixing of an ethanolic solution of H_2L with $Dy(NO_3)_2$·6H_2O and $Y(NO_3)_2$·6H_2O in the adequate molar ratios, yields a red solid that could not be satisfactorily characterized. The same occurs if the initial ligand solution is basified with Me_4NOH up to operational pH = 9.5, and then mixed with the solution of dysprosium and yttrium salts. However, when the same reaction is repeated, but the solution of H_2L is basified with two equivalents of Et_3N, the complex Et_3N[$Dy_{0.09}Y_{0.91}(L)(NO_3)_2$] (**4**) is isolated in the form of single crystals. Nevertheless, the multiple attempts made by varying the operational pH of the medium with either Me_4NOH or Et_3N did not allow obtaining the desired [$Dy_{0.09}Y_{0.91}(HL)(NO_3)_2$] compound.

Single crystals of **1**·Py·0.5CH_3OH·0.5H_2O, **2**·2H_2O and **3** were also obtained, by recrystallization of **1**·H_2O from a solution of pyridine/methanol/toluene by diffusion of diethylether, directly from slow evaporation of the mother liquor of **2**·2H_2O, or by recrystallization of solid **3** in methanol/hexane.

The complexes were unequivocally characterized by microanalysis and IR spectroscopy. In addition, **1**·Py·0.5CH_3OH·0.5H_2O, **2**·2H_2O, **3** and **4** were studied by single X-ray diffraction studies. Besides, the magnetic behavior of **1**·H_2O-**4** was also analyzed.

The infrared spectra of **1**·H_2O, **2**·2H_2O and **3** show two intense bands at *ca*. 1585 and 1540 cm^{-1}, assigned to ν(C=N) vibrations of the imine and pyridine moieties, respectively.[40] These bands undergo negative shifts ranging from 37 to 51 cm^{-1} respect to the free ligand, indicating that both the imine and pyridine nitrogen atoms are coordinated to the metal ion. The spectra of **1**·H_2O and **2**·2H_2O also show two strong bands at *ca*. 1270 and 1460 cm^{-1}, in agreement with

the presence of nitrate groups coordinated in a bidentate fashion.[40] In addition, these spectra present broad bands in the range 3200-3600 cm^{-1}, which agree with the existence of coordinated or solvated water and/or ethanol. In the case of **3**, the spectrum shows one quite sharp band at 3327 cm^{-1}, in accordance with the presence of the non-deprotonated alcohol function of the hemiacetal group.

X-ray diffraction studies

[Dy(HL)(NO$_3$)$_2$]·Py·0.5CH$_3$OH·0.5H$_2$O (1·Py·0.5CH$_3$OH·0.5H$_2$O). An ellipsoid diagram for **1** is shown in Figure 1, and main distances and angles are given in Table S2. The unit cell of **1**·Py·0.5CH_3OH·0.5H_2O contains neutral [Dy(HL)(NO_3)$_2$] molecules, in addition to pyridine, and disordered methanol and water as solvates.

In [Dy(HL)(NO_3)$_2$], the monoanionic HL^- Schiff base acts as a pentadentate N_3O_2 donor. In spite of the conjugation and, therefore, nearly planar character of the ligand, it adopts a helical disposition in this complex. Hence, the oxygen atoms O1 and O2 are the ones that deviate most from the mean N_3O_2 calculated plane, and they are *ca*. 0.391 Å above or below this mean plane.

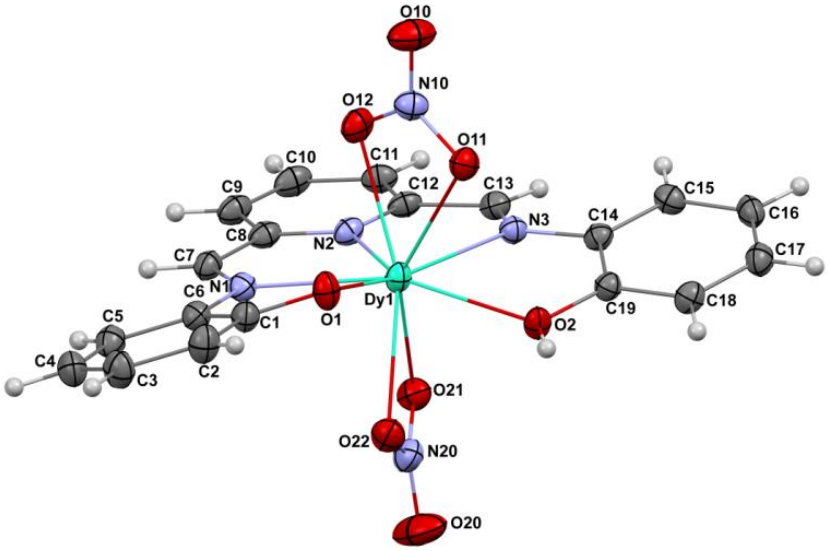

Figure 1. Ellipsoid (50% probability) diagram for **1**.

The coordination sphere of the dysprosium atom is completed by two nitrate ligands, acting as bidentate chelate donors, which are rotated with respect to each other, in such a way that the

NO_2 calculated planes form an angle of *ca*. 60.8º. Consequently, the dysprosium center has coordination number 9. Calculations of the degree of distortion of the DyN_3O_6 core with respect to an ideal nine vertex polyhedron with the SHAPE software,[41] gives rise to shape measurements closer to spherical tricapped trigonal prism (Figure 2, Table S3).

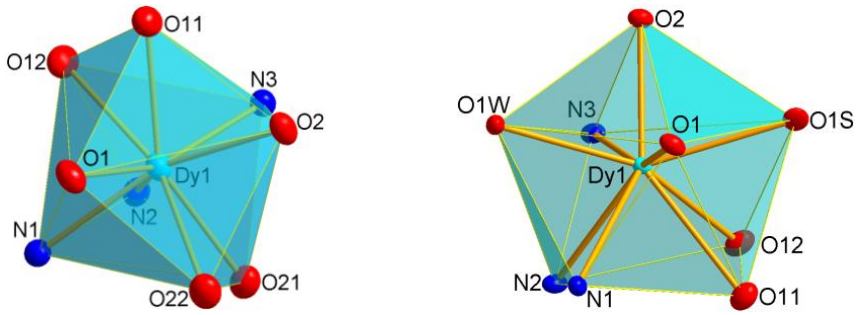

Figure 2. Coordination environments for the Dy^{III} ions in **1** (left) and **2** (right), showing the distorted spherical tricapped trigonal prism, and spherical capped square antiprism structures.

All the bond distances and angles about the dysprosium(III) ion are in their normal ranges.[14-16] However, it should be noticed that the Dy1-O2 distance is significantly longer than the Dy1-O1 bond length, which is in agreement with the monodeprotonation of the Shiff base, where O2 remains protonated.

The $[Dy(HL)(NO_3)_2]$ molecules in the cell are quite far away, and the shortest intermolecular Dy···Dy distance is 8.1294(7) Å

[Dy(L)(NO₃)(EtOH)(H₂O)] (2·2H₂O). The unit cell of **2**·$2H_2O$ contains $[Dy(L)(NO_3)(H_2O)(EtOH)]$ molecules (Figure 3) and water as solvate. The structure of $[Dy(L)(NO_3)(H_2O)(EtOH)]$ is quite similar to that of $[Dy(HL)(NO_3)_2]$, but with some significant differences. Thus, in the same way as in **1**, the Schiff base, which now is dianionic, acts as a pentadentate N_3O_2 donor. Nevertheless, the multidentate ligand has now an umbrella like distortion, with the dysprosium atom *ca*. 0.42 Å above the mean calculated N_3O_2 plane.

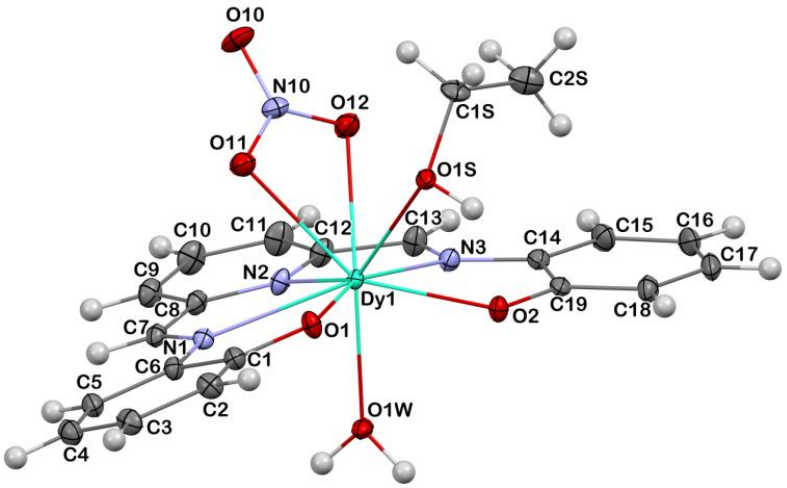

Figure 3. Ellipsoid (50% probability) diagram for **2**.

The coordination sphere about Dy^{III} is completed by a bidentate chelate nitrate donor, one water and one ethanol molecule, leading to coordination number 9. In this case, calculations of the distortion from an ideal DyN_3O_9 core with the SHAPE program indicate that the geometry is closer to spherical capped square antiprism, but highly distorted towards muffin (Figure 2, Table S3). The main distances and angles about the metal center agree with those expected for this kind of compound,[14-16] but it should be mentioned that the distances Dy1-O1 and Dy1-O2 are quite similar, and shorter than Dy1-O2 in complex **1** (Table S2). This clearly suggests that in **2** both phenolic oxygen atoms are deprotonated.

Finally, it should be noted that the phenolic oxygen atoms, the nitrate ligand, coordinated water and ethanol, and water solvates are implicated in a complex hydrogen bond scheme, which expands the initial molecule into a 3D grid, where the shortest intermolecular Dy···Dy distance is 6.4395(5) Å.

[Dy(HL')$_2$)][Dy(L)(Cl$_2$)] (3). An ellipsoid diagram for **3** is shown in Figure 4 and main distances and angles are recorded in Table S4.

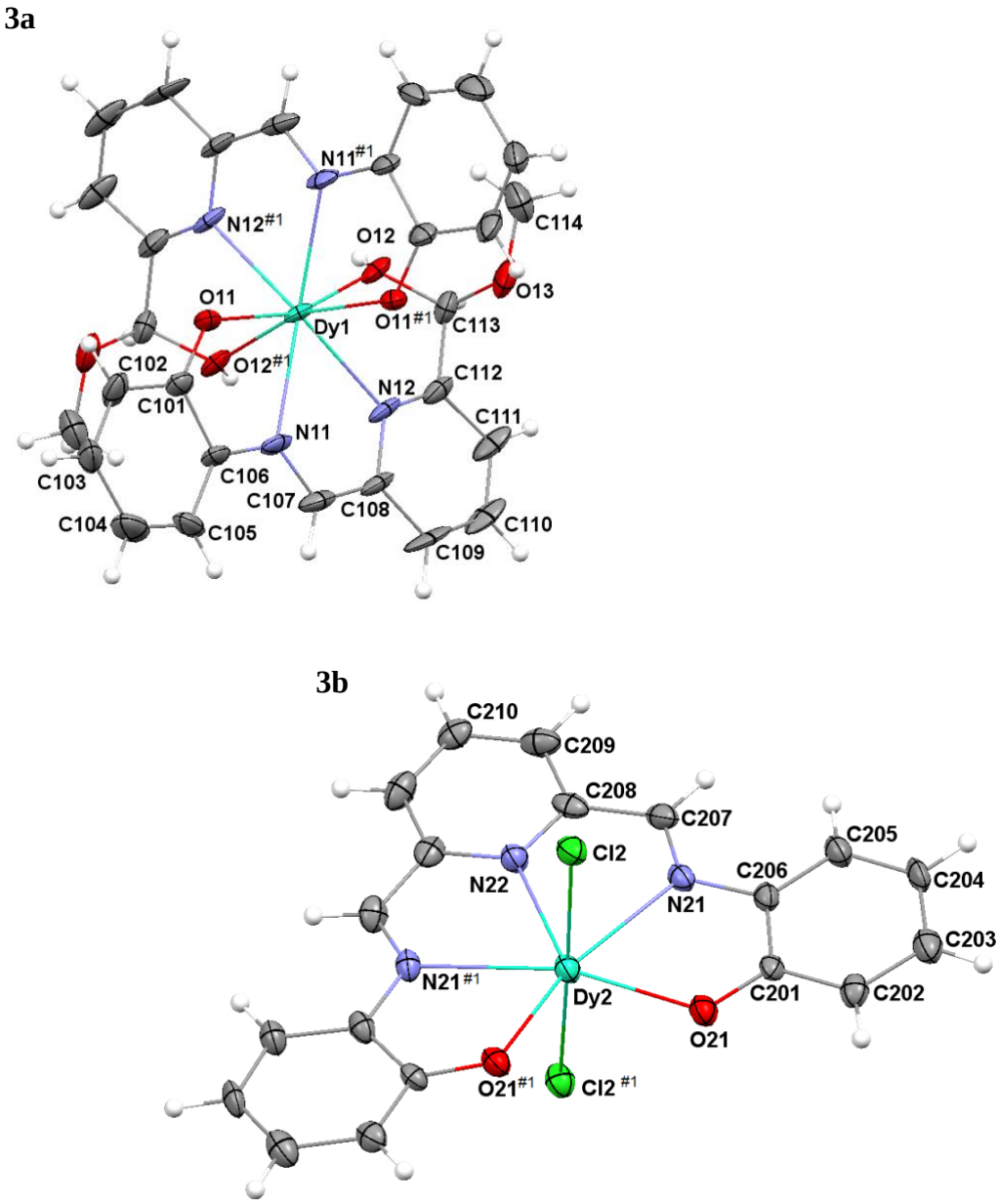

Figure 4. Ellipsoid (30% probability) diagram for **3**: top) cation **3a**; bottom) anion **3b**

The crystal structure of **3** shows that it is an ionic compound, composed of $[Dy(L^{'})_2)]^{+}$ cations (**3a**) and $[Dy(L)(Cl_2)]^{-}$ anions (**3b**). In the **3a** cation (Figure 4), the dysprosium ion is surrounded by two imine-hemiacetal ligands that act as monoanionic N_2O_2 donors, linking the metal ion through the nitrogen atoms of the imine and pyridine functions, the deprotonated phenolic oxygen atom, and the protonated alcoholic oxygen atom of the hemiacetal group. Accordingly, the dysprosium ion is octacoordinated in an N_4O_4 environment, with a calculated geometry closer to triangular dodecahedron, but distorted towards snub diphenoid (Table S3,

Figure 5).[41] The cation has two chiral centeres, the carbon atoms of the hemiacetal groups, but both *S*,*S* and *R*,*R* isomers of the **3a** cation are present in the unit cell in 1:1 ratio, thus giving rise to a racemic mixture.

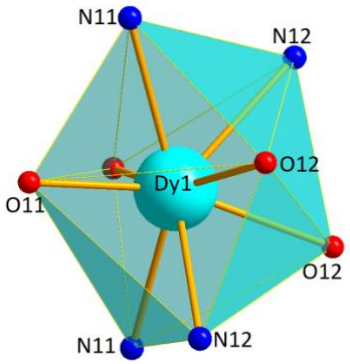

Figure 5. Distorted triangular dodecahedron coordination environment for Dy^{III} in **3a**.

In the **3b** anion (Figure 4), the bisdeprotonated Schiff base L^{2-} wraps the dysprosium(III) center in its N_3O_2 pocket, as in **1** and **2**. The coordination sphere is completed by two chloride anions, and, accordingly, the dysprosium ion achieves coordination number 7, with slightly distorted pentagonal bipyramid geometry (Table S3, Figure 4). In this case, the pentadentate donor is nearly planar (maximum deviation of any atom from the mean calculated N_3O_2 plane of 0.112 Å, with the Dy atom in the plane), and the Cl-Dy-Cl angle is *ca*. 177º.

Besides, this structure is further stabilized by two short hydrogen bonds (O···O distances of *ca*. 2.5 Å) between the phenolic oxygen atoms of the **3b** anion and the protonated alcoholic functions of the **3a** cation, what generates a pseudodinuclear complex, with a $Dy^{III}\cdots Dy^{III}$ distance of *ca*. 5.486 Å (Figure S1).

(Et$_3$NH)[Dy$_{0.09}$Y$_{0.91}$(L)(NO$_3$)$_2$] (4). An ellipsoid diagram of the compound is shown in Figure S2, and main distances and angles in Table S5. In this case the complex is also ionic, the $[Dy_{0.09}Y_{0.91}(L)(NO_3)_2]^-$ anion and Et_3NH^+ cation being joined through a hydrogen bond between the nitrogen atom of the cation and one phenolic oxygen atom of the anion. No other hydrogen bonds are observable in the cell, and the shortest distance between dysprosium or yttrium atoms of two neighbouring $[Dy_{0.09}Y_{0.91}(L)(NO_3)_2]^-$ anions is *ca*. 8.36 Å.

The structure of the $[Dy_{0.09}Y_{0.91}(L)(NO_3)_2]^-$ complex is similar to that described for $[Dy(HL)(NO_3)_2]$, but with one remarkable difference: the Schiff base is in this case bisdeprotonated, with both phenol oxygen atoms negatively charged. Thus, as in **1**, in the $[Dy_{0.09}Y_{0.91}(L)(NO_3)_2]^-$ anion the pentadentate ligand also adopts a helical disposition, and the calculated environment around the yttrium and dysprosium ions with the SHAPE program is closer to spherical tricapped trigonal prism. Therefore, as all the distances and angles are in the expected range, this structure does not deserve further discussion.

Moreover, powder X-ray diffraction studies were recorded for the crude products **2**·$2H_2O$ and **3**. In the case of **2**·$2H_2O$, the aim of this study is to demonstrate that the microcrystalline product and the single crystals are the same compound, given that single crystals of **2**·$2H_2O$ have been obtained from the mother waters. The X-ray diffraction pattern of this microcrystalline powder was compared with the calculated one using the single X-ray diffraction data of **2**·$2H_2O$ (Figure S3), and these studies show that the solid and the crystals from the mother liquor are exactly the same compound, and that **2**·$2H_2O$ has been obtained with high purity, being the only product in the crude microcrystalline sample.

Powder X-ray diffractograms for two microscrystalline samples of **3**, obtained from two different syntheses, were recorded (Figure S4). This study was done in order to demonstrate that **3** is the only product in the solid sample, and not a byproduct generated in the recrystallisation process, and that the experiment is reproducible and not just the result of serendipity. When these diffractograms were compared with the calculated one using the single X-ray data (Figure S4), it could be concluded that both microcrystalline samples are exactly the same compound, thus demonstrating that the experiment is reproducible, and that they are the same product as the one crystallographically solved.

At this point, it must be highlighted that complexes **1**-**4** are the first lanthanoid compounds of H_2L and related ligands to be crystallographically characterized. Accordingly, some main

group or d-metal complexes derived from H_2L type ligands were previously crystallographically solved (Table 1) but, up to now, and as far as we know, no crystal structures for lanthanoid complexes of H_2L were reported. A search from CSD data[42] (Table 1) shows that this type of ligand can usually act as dianionic, which is its most common charge, or as a neutral Schiff base, but it has only been described once as a monoanionic donor to date.

Table 1. Metal complexes derived from H_2L and related ligands crystallographically solved.

Metal complex[a]	Charge/ Coordination mode[b]	Nuclearity	Ref.
$[Cd_3L(OAc)_2(dmf)_2]$	dianionic/N_3O_2 μ_2-bridge	trinuclear	43
$[ReL(PPh_3)_2]I$	dianionic/N_3O_2 chelate	mononuclear	44
fac-$[Re(CO)_3H_2L(Br)]$	neutral/N_2 chelate	mononuclear	44
fac-$[Re(CO)_3H_2L(Cl)]$	neutral/N_2 chelate	mononuclear	45
$[SnL(Bu^n)_2]$	dianionic/N_3O_2 chelate	mononuclear	24
$[SnL(Ph)_2]$	dianionic/N_3O_2 chelate	mononuclear	24
$[Mn(H_2L)Cl_2]$	neutral/N_3O_2 chelate	mononuclear	46
$[Mn_2Ca(L)_2(OAc)_2(MeOH)_2]$	dianionic/N_3O_2 μ_2-bridge	trinuclear	46
$[Mn_3(L)_2(OAc)_2(MeOH)_2]$	dianionic/N_3O_2 μ_2-bridge	trinuclear	46
$[Zn_2(L)(OAc)_2(DMF)]$	dianionic/N_3O_2 μ_2-bridge	dinuclear	47
$[Zn_4(5\text{-}Bu^tL)_2(OAc)_4]$	dianionic/N_3O_2 μ_4-bridge	tetranuclear	47
$[Zn(3\text{-}MeH_2L)(Cl)_2]$	neutral/N_2O chelate	mononuclear	48
$[Zn_2(5\text{-}MeL)(Cl)_2(MeOH)_2]$	dianionic/N_3O_2 bridge	dinuclear	48
[Mn(5-MeHL)(Cl)(MeOH)]	monoanionic/N_3O_2 chelate	mononuclear	49
$[Sn(5\text{-}MeL)(Bu^n)_2]$	dianionic/N_3O_2 chelate	mononuclear	24
$[Mn(H_2L^1)(NCS)_2]$	neutral/N_3O_2 chelate	mononuclear	49
$[Cd_4(L^{Me})_2(OAc)_4]$	dianionic/N_3O_2 μ_4-bridge	tetranuclear	43,47
$[Sn(L^{Me})(Bu^n)_2]$	dianionic/N_3O_2 chelate	mononuclear	24
$[Sn(L^{Me})(Me)_2]$	dianionic/N_3O_2 chelate	mononuclear	24
$[Mn_4(L^{Me})_2(OAc)_4]$	dianionic/N_3O_2 μ_4-bridge	tetranuclear	50
$[Mn_4(L^{Me})_2(CF_3COO)_4]$	dianionic/N_3O_2 μ_4-bridge	tetranuclear	50
$[Zn_4(L^{Me})_2(OAc)_4]$	dianionic/N_3O_2 μ_4-bridge	tetranuclear	47
$[Zn_4(L^{Me})_2(OAc)(O_2CC_6H_5)_3]$	dianionic/N_3O_2 μ_4-bridge	tetranuclear	47
$[Zn_4(5\text{-}ClL^{Me})_2(OAc)_4]$	dianionic/N_3O_2 μ_4-bridge	tetranuclear	47

[a] Complexes without solvates; ligands in Scheme 3 (except H_2L, Scheme 1); [b] coordination mode in Scheme 4

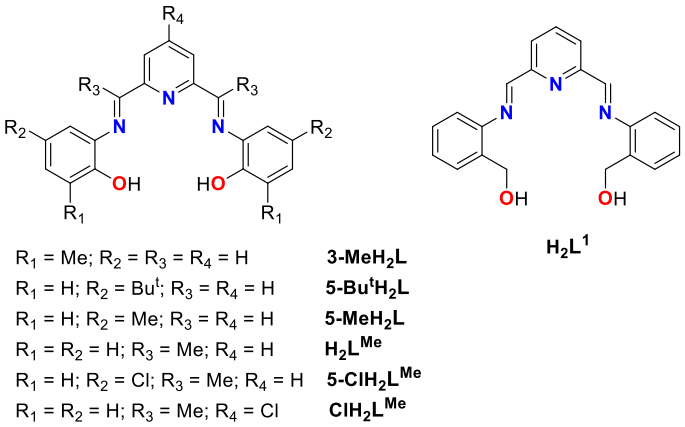

Scheme 3. Related ligands of H_2L in crystallographically solved complexes.[24, 43-50]

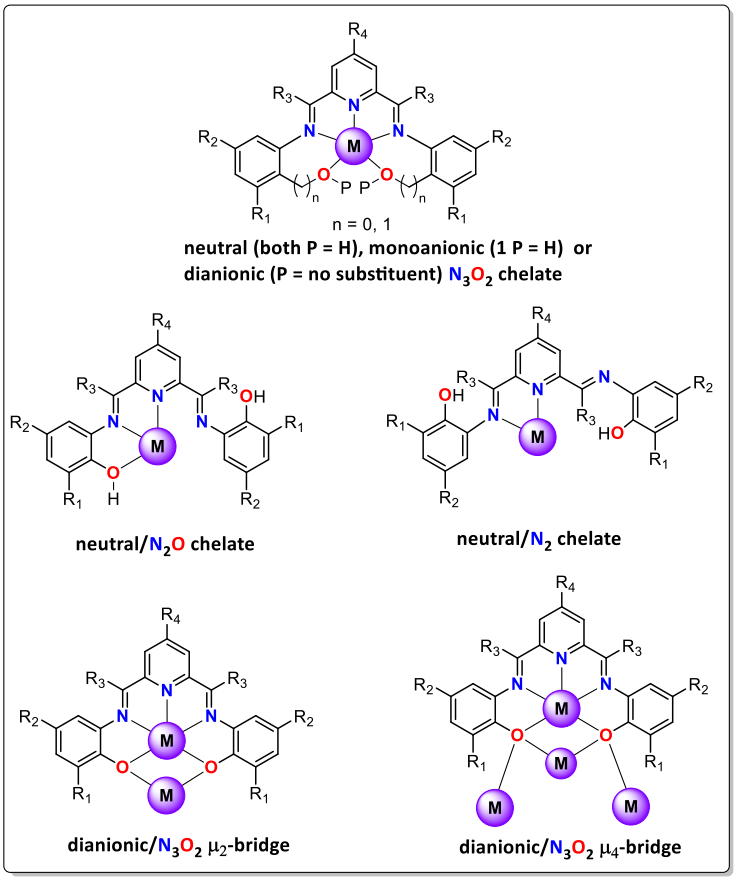

Scheme 4. Coordination modes shown by the ligands of Schemes 1 and 3 in metal complexes.

In its dianionic form, the most common coordination modes are as a pentadentate bridge, using the three nitrogen atoms to bind a metal center, and the phenolic oxygen atoms to bridge two or more metal ions, or as an N_3O_2 non-bridging chelating donor (Scheme 4). This latter one is the coordination mode found in all the lanthanoid complexes described herein, and it

should be noted that the degree of deprotonation of the ligand found in **1** (monodeprotonated) is unique for H_2L.

Thus, the structural features observed for **1**-**4** show that the chelating pentadentate H_2L wraps the metal center forming a more or less distorted plane. The deviation from planarity seems to be related with the number and nature of the auxiliary ligands. Accordingly, the presence of chloride promotes a nearly perfect equatorial N_3O_2 plane, with just two auxiliary ligands in the apical sites, as it can be seem in **3b**. Thus, this leads to minor distortion of the pentagonal bipyramidal geometry. Consequently, the structural studies reported in this work open a door for the rational design of lanthanoid complexes with predetermined pentagonal bipyramidal environments in the presence of auxiliary donors of different nature.

Magnetic Properties. Direct-current (dc) magnetic susceptibility measurements were recorded for **1**·H_2O, **2**·$2H_2O$ and **3** as a function of the temperature. The plots of $\chi_M T$ *vs* *T* for **1**·H_2O, **2**·$2H_2O$ and **3** are shown in Figure 4, and Figures S5 and S6, respectively.

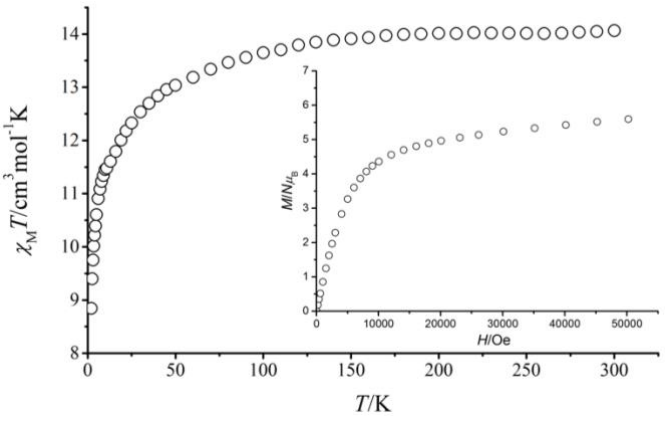

Figure 4. $\chi_M T$ *vs* *T* for **1**·H_2O. Inset: $M/N\mu_B$ *vs* *H*.

At 300 K, the $\chi_M T$ values are 14.07 cm^{3}Kmol^{-1} for **1**·H_2O, 14.13 cm^{3}Kmol^{-1} for **2**·$2H_2O$ and 29.3 cm^{3}Kmol^{-1} for **3**, values that are very close to those expected for one or two isolated Dy^{3+} ions (14.13 cm^{3}Kmol^{-1} per ion). In all cases, the experimental $\chi_M T$ values remain almost constant when the temperature decreases up to 70 K. Below this temperature, the drop in the

curves is more pronounced, and the molar susceptibilities reach minimum values of 8.84, 7.83 and 18.01 cm^3kmol^{-1} at 2 K for **1**·H_2O, **2**·$2H_2O$ and **3**, respectively. This drop can be mainly ascribed to depopulation of the M_J sublevels of the dysprosium(III) ion at low temperatures. Nevertheless, in the case of **3**, the drop below 13 K is even more marked and maybe the intermolecular interactions through the short hydrogen bonds between the anion and the cation play a role in this strong diminishment of the $\chi_M T$ value.

The reduced magnetization at 2 K tends to 5.59 $N\mu_B$ for **1**·H_2O, 6.35 $N\mu_B$ for **2**·$2H_2O$ and 10.45 $N\mu_B$ for **3** at maximum applied field of 5 T (Figure 4, S5 and S6, inset). These values are considerable smaller than those expected for one or two isolated Dy^{III} centers (10 $N\mu_B$ per Dy^{III} ion), but comparable with the values reported for many complexes per dysprosium center,[16,51-54] what seems to agree with a significant magnetic anisotropy.

The low-temperature magnetic relaxation behavior of complexes **1**·H_2O-**3** was studied. Thus, alternating current (ac) magnetic susceptibility measurements were initially recorded under a zero external field at a frequency of 1400 Hz. In this case, none of the compounds show out-of-phase ac susceptibilities (χ''_M) peaks. However, it is well known that these molecules can present quantum tunnelling (QTM) relaxation processes,[55] which prevent to observe the SMM behavior. One way to partly or fully suppress this quantum tunnelling is the application of a small static magnetic field,[56] which should remove the mixing of the ground $\pm M_J$ levels, thus enabling observation of the slow relaxation process through the real thermally activated energy barrier.

Consequently, variable temperature ac susceptibilities were measured with the application of different dc fields. Under these conditions, **1**·H_2O shows ac susceptibility frequency and field dependence below 5 K, but without a maximum in its χ''_M curves (Figure S7). Nevertheless, **2**·$2H_2O$ and **3** show χ''_M peaks as a function of the temperature at fixed frequencies. Accordingly, ac measurements as a function of the frequency at 5 K for **2**·$2H_2O$

and 3K for **3** under different dc fields were performed in order to establish the optimum field (Figures S8 and Figure S9). In this conditions, based on the highest relaxation time, the fields of 1500 Oe and 3000 Oe were chosen as the optimal ones for **2**·2H$_2$O and **3**, respectively.

2·2H$_2$O exhibits frequency and temperature-dependence of the in phase (Figure S10) and out-of-phase (Figure 5) susceptibility under this field of 1500 Oe, with maxima for χ''_M between 4 and 6 K, and, therefore, field-induced SMM-like behavior.

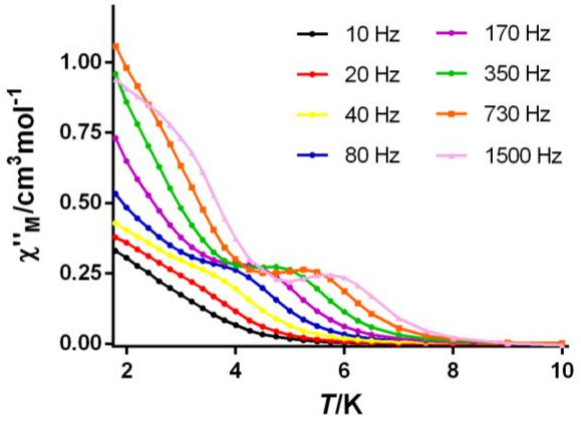

Figure 5. Temperature dependence of χ''_M for **2**·2H$_2$O in a dc applied field of 1500 Oe at different frequencies.

Besides, it should be noted that Figure 5 reveals that χ''_M does not go to zero below the maxima at low temperature, which indicates that the fast relaxation of the magnetization by a QTM mechanism has not been fully suppressed by the application of the optimum magnetic field. In addition, the Cole–Cole plot for **2**·2H$_2$O between 4.5 and 6 K (Figure S11) displays semicircular shapes with α parameters in the range 0.14-0.09 (Table S6), which suggests more than one relaxation process at low temperature.

The relaxation dynamics can be further analysed by studying the temperature dependence of the relaxation time. The Arrhenius plot (Figure 6) shows that the data deviate from linearity in the low-temperature region and, therefore, the curve cannot be reproduced with a simple Orbach model, as expected in view of the α parameter. For this reason, and taking into account the experimentally observed QTM, we have tried to fit this plot taking into account all the

possible relaxation processes in addition to QTM, but equation 1, which includes contributions from quantum tunnelling and Orbach thermal processes, is the one that best simulate this plot rendering reasonable parameters.

$$\tau^{-1} = {\tau_{QTM}}^{-1} + {\tau_0}^{-1} e^{-U_{eff}/k_B T} \quad (1)$$

The best fit with this equation yields an effective energy barrier U_{eff} of 60.47 K, with a τ_0 factor of 5.61×10^{-9} s and τ_{QTM} of 0.374 ms.

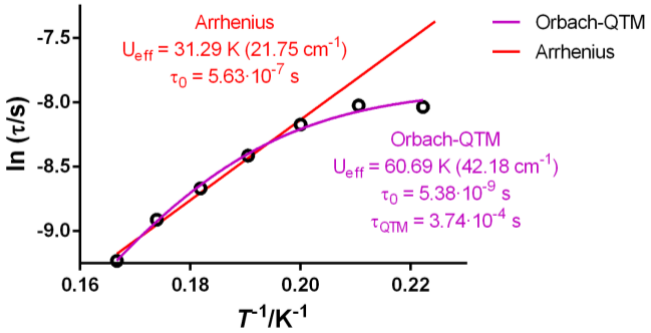

Figure 6. Arrhenius plot for **2**·2H$_2$O in a dc applied field of 1500 Oe. The red line accounts for the best fit considering Orbach plus QTM relaxation (eq. 1).

χ'_M (Figure S10) and χ''_M (Figure 7) for **3** also show temperature and frequency dependence at the optimum external field of 3000 G (Figure S9). The χ''_M plot versus *T* (Figure 7) shows that χ''_M presents some peaks at different frequencies and, as in the case of **2**·2H$_2$O, it shows same tails at low temperature, also indicating the existence of QTM.

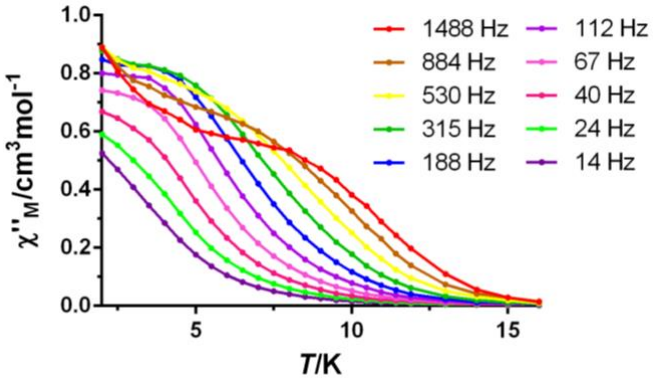

Figure 7. Temperature dependence of χ''_M for **3** in H_{dc} = 3000 Oe at different frequencies.

The fit of the Cole-Cole plot to a generalized Debye model gives α parameters between

0.39 and 0.16 (Table S6), which also agrees with the presence of more than one relaxation process (Figure S12). Thus, Figure 8 shows that the Arrhenius plot does not fit to a simple Orbach model, and that its best fit is achieved with equation 1, yielding values of U_{eff} of 31.02 K, with a τ_0 factor of 4.22×10^{-6} s, and τ_{QTM} of 0.511 ms.

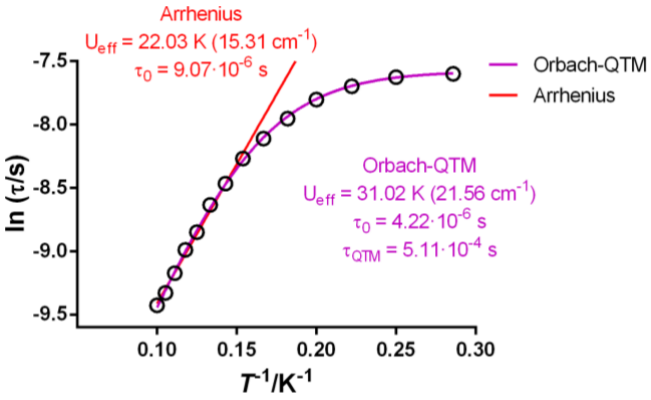

Figure 8. Arrhenius plot for **3** in a dc applied field of 3000 Oe. The violet line accounts for the best fit considering Orbach plus QTM relaxation (eq. 1).

As shown in Figure S7, **1**·H_2O does not show χ''_M peaks as a function of the temperature, but frequency dependence of χ''_M in an external field of 2000 G (Figure S7). This phenomenon might be due to the existence of a very small thermal energy barrier for the reversal of the magnetization to block the magnetization above 2 K, and/or owing to the occurrence of a rapid QTM relaxation process, which the dc field is not able to eliminate. Therefore, efforts were made to know the origin of the non-SMM like behavior for **1**·$2H_2O$ in the presence of a dc field. Thus, if this behavior were attributable to a QTM effect caused by intermolecular dipolar interactions, these usually could be removed by diluting the sample with a diamagnetic matrix.[50] Accordingly, attempts to prepare the diluted yttrium complex $[Dy_{0.09}Y_{0.91}(HL)(NO_3)_2]$ were made. However, as it was discussed, these endeavors lead to the isolation of $(Et_3NH)[Dy_{0.09}Y_{0.91}(L)(NO_3)_2]$ (**4**), crystallographically solved, but the desired compound could not be obtained regardless of the multiple attempts.

Likewise, the dynamic magnetic properties of **4** were studied (Figures 9 and S13). It should

be noted that for **4** χ'_M shows dependence of the frequency and temperature (Figure S13), and χ''_M shows peaks as a function of the temperature and frequency in the absence of an external dc field (Figure 9). Nevertheless, the tail of this curve does not tend to zero, indicating that the QTM is still efficient at a zero field, in spite of the diluted nature of the sample. Fitting the Cole−Cole plots to the generalized Debye model gives a series of α parameters below 0.41 (Figure S14, Table S6), indicating a very narrow distribution of relaxation times in a single relaxation process.

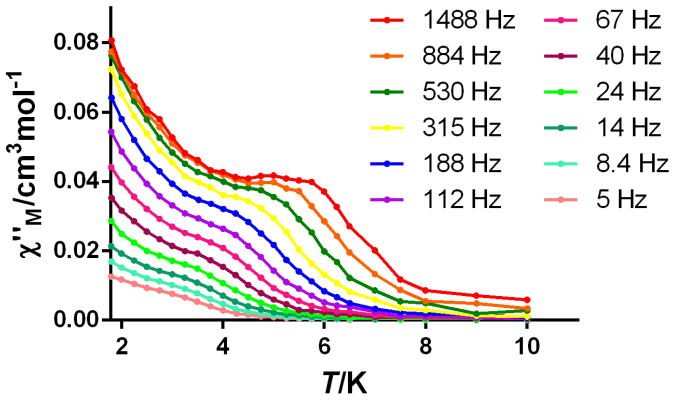

Figure 9. Temperature dependence of χ''_M for **4** in a dc zero field at different frequencies.

Consequently, many attempts were made to fit the Arrhenius plot but, once again, the best fit with coherent parameters was found with equation 1 (Figure 10), giving values of U_{eff} = 49.10 K (34.13 cm^{-1}), τ_0 = 3.635 x10^{-8} s, and τ_{QTM} = 0.184 ms.

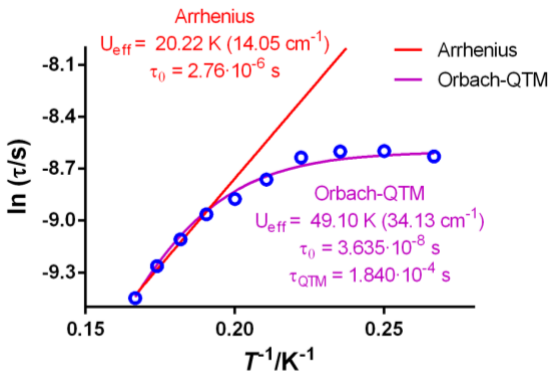

Figure 10. Arrhenius plot for **4** in a zero dc applied field. The violet line accounts for the best fit considering Orbach plus QTM relaxation (eq. 1).

The ac magnetic susceptibility data for **4** were additionally measured in the presence of an applied field of 1500 Oe, in order to shortcut the quantum channel (Figures 11 and S13).

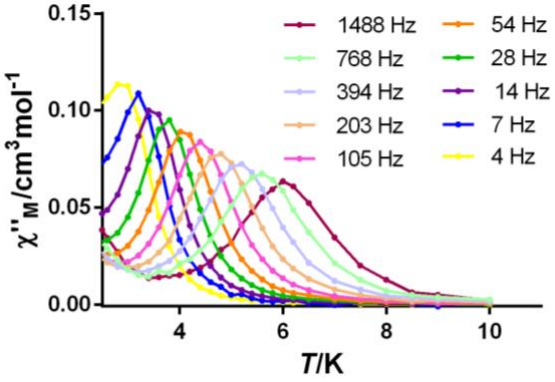

Figure 11. Temperature dependence of χ''_M for **4** in a dc applied field of 1500 Oe at different frequencies.

The Arrhenius plot extracted from these data can only be fitted with equation 2 (Figure 12), which considers Orbach and Raman effects, and that agrees with the presence of more than one relaxation process suggested by the Cole-Cole plot fitting (α = 0.18-0.14, Figure S14, Table S6). The best fit yields basically the same U_{eff} value (50.12 K, 34.83 cm^{-1}) as in the absence of dc field, with an enhanced relaxation time of 5.11 x10^{-8} s.

$$\tau^{-1} = CT^{-n} + {\tau_0}^{-1}\mathrm{e}^{-U_{eff}/k_B\mathrm{T}} \quad (2)$$

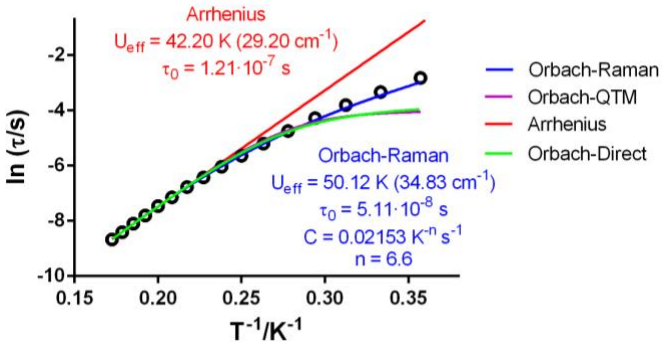

Figure 12. Arrhenius plot for **4** in a dc applied field of 1500 Oe. The colored solid lines accounts for the best fit considering different relaxation processes.

The n value of 6.6 extracted from this fit could seem lower than the expected one for Dy^{III} (n = 9), but it is within the typical range of 5-9 found for many other dysprosium(III) complexes.[57]

Electronic Structure calculations. CASSCF calculations by including spin-orbit effects with the RASSI approach (see Computational details section) were employed in order to explain the magnetic properties of the synthesized compounds. Due to the relatively large ionic character of the dysprosium-ligand bonds, and the large number of unpaired electrons, dynamic correlation effects are not crucial to describe such systems.[58-60] We have considered six molecular structures **1** with (**1w**) and without (**1wo**) the pyridine molecule, **2**, **3** (the **3c** cation and **3a** anion) and **4** (see Figure 13). The methodology that was widely employed to study this kind of systems[60-62] provides a reasonable agreement with the experimental susceptibility and magnetization curves (see Figs. S15 and S16).

The main calculated parameters for the six systems are collected in Table 2. As expected, from the calculated g-factors all these Dy^{III} systems present easy-axis character. The direction of the easy axis is determined by the spatial distribution of the ligands. The oblate shape of the electron density expected for Dy^{III} center ($^6H_{15/2}$ m_J = 15/2 ground state) is an axially-compressed disc that is accommodated in the molecules to reduce the metal-ligand electrostatic repulsion.[58,59] It is worth noting that both **1** systems are those showing the largest axial character from the calculated g values. Furthermore, also the energies are consistent with such conclusion. The excitation energies without spin-orbit contribution indicate the degree of mixing of the excited states with the ground state when the spin-orbit coupling is included. Previously,[59,60] some of us noticed that the figure of merit of the axiality is $(E_2-E_1)/E_1$. Large $(E_2-E_1)/E_1$ values results in large anisotropy because the first excited state has a relatively large axial character, like the ground state, but the second excited state is much less axial (see representation of the beta electron densities in Figs. S17 and S18). Thus, first excitation energy

for complex **1** is similar to that of the other systems while the second excitation energy is almost twice than in the other systems (see Table 2). **3b** is slightly different to the other complexes, due to the presence of two chloride anions with weaker ligand field and furthermore, the equatorial ligand is almost perfectly flat while in the other complexes such ligand is slightly distorted (see Figure 1).

Table 2. Calculated first and second excitation energies with (E_{SO}) and without (E) spin-orbit effect (cm^{-1}) and g-factors of the ground and first excited states for six studied molecules.

Compound	E	E_{SO}	g_z	g_y	g_x
1w	10.4	173.2	19.650	0.030	0.017
	247.0	301.5	17.474	0.368	0.319
1wo	11.1	186.3	19.662	0.029	0.013
	260.8	299.9	17.373	0.378	0.313
2	5.5	55.8	18.627	0.079	0.024
	100.9	195.2	16.020	0.060	0.004
3a	22.0	27.5	14.722	3.839	0.692
	105.7	103.4	12.647	4.343	0.479
3b	7.2	107.1	19.448	0.068	0.027
	42.0	140.9	13.300	2.376	0.927
4	17.3	82.2	18.881	0.137	0.052
	112.8	180.6	16.349	0.673	0.566

The magnetic properties are closely related with the adopted structures by these compounds. Thus, if there is a shortest metal-ligand bond distance, the oblate density is perpendicular to such bond to reduce the metal-ligand electron repulsion and consequently, the easy axis is approximately aligned with such bond (see Figs. 13, S17 and S18).

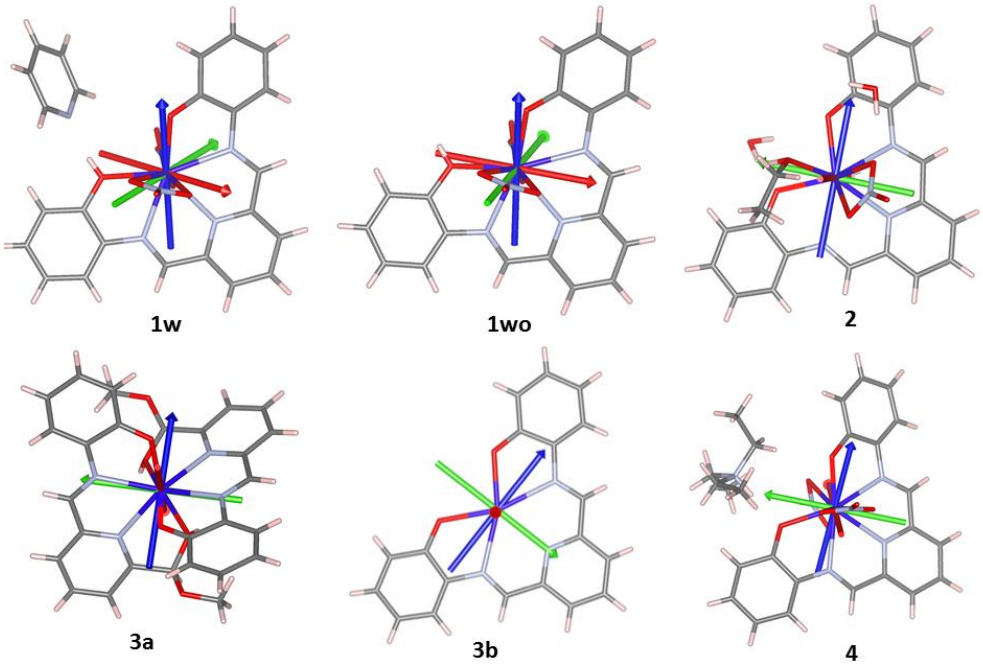

Figure 13. Representation of the directions of the g components for the six calculated systems. The easy axis direction is represented with the blue arrow. Green and red arrows indicate the direction of the g_y and g_x components.

The analysis of the shapes of the beta density of the lowest manifold states at CASSCF level without spin-orbit effect (see Figs. S17 and S18) gives a qualitative picture of the oblate character of the electron density. A weighted mixing of such spin-free states induced by the spin−orbit coupling will result in the ground state of the system that will determine the magnetic properties. In Figure 13, the orientations of the *g*-components are represented for the six systems. For **1**, the shortest metal-ligands bonds are those through the non-protonated phenolic group. Thus, for the two **1** cases, the easy-axis is almost perfectly aligned with the shortest Dy-O bond (2.240 Å bond distance) of the unique non-protonated phenolic group (see Figure 1). However, for the other compounds there are always two non-protonated phenolic groups with the shortest metal-ligand distances and the O-Dy-O bond angles are close to 90º (95.2, 95.2 and 102.4º respectively for **2**, **3a** and **4**). Hence, the oblate disc cannot be easily accommodated with these two oxygen atoms with the shortest Dy-O distances resulting in a decrease of the axial character of the ground state. The **3b** molecule has easy-axis character placed in the plane

of the flat equatorial ligand (see Figure 1) and the oblate electron density (see Figure S4) has less metal-ligand repulsion than in the other complexes with more distorted structures, thus, this system has a larger axiality than the other molecules with two shortest Dy-O distances.

The results show that the presence of only one non-protonated phenolic group as shown in compound **1** favors axiality because the electron density is easier to accommodate. However, **1**·H_2O does not show a maximum in χ''_M. To gain more insight into the relaxation paths of these compounds the qualitative ab initio blocking barrier has been computed (Figure 14).

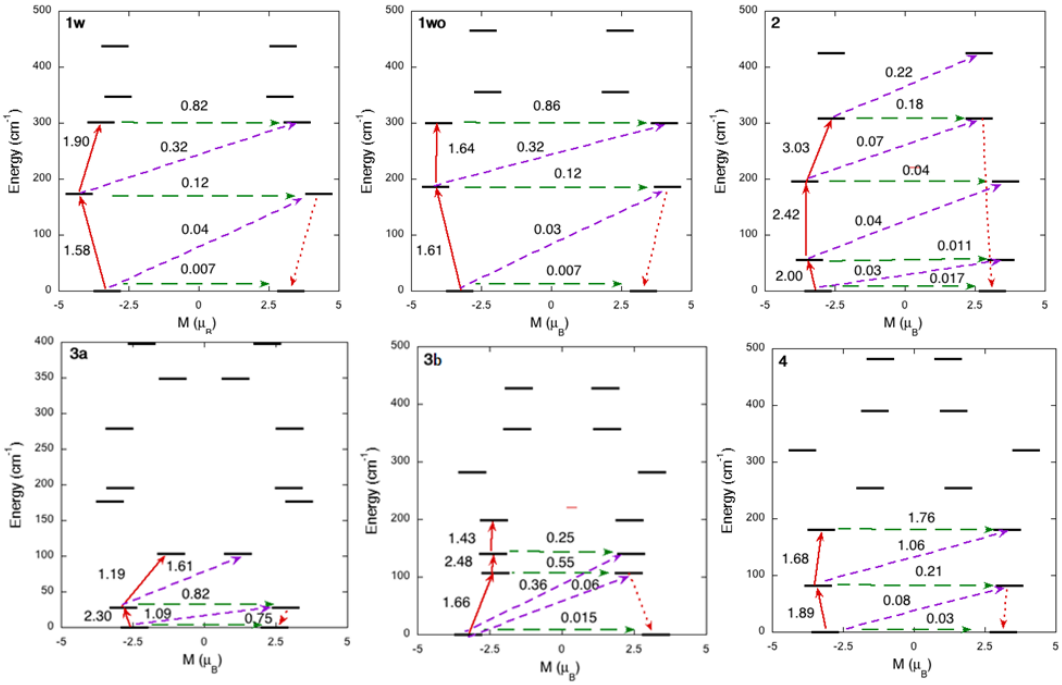

Figure 14. States energies as a function of their average magnetic moment, M, along the main anisotropy axis for six studied systems. The dashed green arrows correspond to the quantum tunneling mechanism of ground or excited states, dashed purple arrow shows the hypothetical Orbach relaxation process. The solid red arrow indicates the transition between the ground and excited Kramers doublets and the dashed red arrow the deexcitation pathway to the ground state with the reversed spin. The values close to the arrows indicate the matrix elements of the transition magnetic moments[32] (above 0.1 an efficient spin relaxation mechanism is expected, see Computational details).

In compound **1**, the tunneling probability between the first excited states is large due to its

axiality, which gives to a faster relaxation than in less axial compounds. This might be the reason for the non-observation of a maximum in χ''_M for this compound. In the case of **2**, however, the relaxation takes place through the third excited state at more than 300 cm^{-1}, and having the largest barrier in the studied compounds. Due to the complexity of compound **3**, it is more difficult to rationalize its behavior, given that it is formed by two species, **3a** and **3b**. The computational results of both of them individually show an efficient relaxation through the first excited states, which in these cases are relatively close to the ground state. However, the interaction between the complexes can have a very important impact in the relaxation processes, which may explain the different observed experimental behavior. Compound **4** also shows and efficient relaxation via tunneling through the first excited state.

When these data are compared with the experimental results, the same trends are not observed, but this is due to different factors. First of all, the complexity of **3** makes it difficult to extract valid correlations from their units **3a** and **3b**. In addition, compound **4** is the only one that is magnetically diluted, thus avoiding dipolar interactions that can suppress the relaxation trough tunnelling.[63] However, the computational results can explain the observed differences between **1** and **2**, and these lead to conclude that the lack of maximum in χ''_M for **1** in spite of its larger axiality can be due to the more efficient relaxation processes.

CONCLUSIONS

This work reports the study of the coordination chemistry of dysprosium(III) nitrate and dysprosium(III) chloride with the well-known H_2L ligand, showing that this chemistry is greatly influenced by the operational pH of the medium, and/or by the anion present in metal salt. Thus, mixing of dysprosium(III) nitrate with H_2L allows to obtain and crystallographically characterize two different neutral nitrate complexes, where the Schiff base ligand remains intact. Nevertheless, the reaction with dysprosium(III) chloride leads to isolate an ionic chloride

complex, where the cation shows that the ligand has partially hydrolyzed, and formed an hemiacetal function, a reaction that has been scarcely reported in literature. These complexes constitute the first lanthanoid compounds derived from H_2L to be crystallographically solved. The crystallographic studies show that the ligand acts as a chelating pentadentate nearly flat donor in **1** to **3**, and in the homologous diluted complex $(Et_3NH)[Dy_{0.09}Y_{0.91}(L)(NO_3)_2]$ (**4**). The crystal structure of **3** demonstrates that the ligand can predetermine a pbp geometry around Dy^{III} in the presence of more or less bulk auxiliary donors. Full magnetic characterization of **1**·H_2O, **2**·$2H_2O$ and **3** reveals that **2**·$2H_2O$ and **3** are field induced SIMs, the largest effective energy barrier of 60.47 K being achieved by **2**·$2H_2O$. However, **1**·H_2O only shows frequency dependence of χ''_M in an external field of 2000 G, but not SIM behavior could be demonstrated. This difference in slow relaxation of the magnetization is explained in light of *ab initio* calculations, which demonstrated more axiality for **1** but also more efficient relaxation pathways through a tunneling mechanism. In the case of **3**, the presence of two different complexes in the molecule prevents any correlation with **1**·H_2O and **2**·$2H_2O$. Diluted sample **4** is a SIM, showing slow relaxation in the absence of a dc field. This fact seems to indicate that maybe the non-observation of SIM behavior for **1**·$1H_2O$ and **2**·$2H_2O$ at $H_{dc} = 0$ could be related to dipolar interactions. Further experiments are being carried out in our lab with this ligand, in order to introduce sterically demanding ligands in apical positions, which should lead to pentagonal bipyramidal mononuclear complexes with increased U_{eff} barriers and blocking temperatures.

ASSOCIATED CONTENT

Supporting Information

Crystallographic data (CIF) for **1**·Py·$0.5CH_3OH$·$0.5H_2O$-**4**, Figures S1-S14 and Tables S1-S6. This material is available free of charge via the Internet at http://pubs.acs.org.

AUTHOR INFORMATION

Corresponding Author

Corresponding Author: *E-mail: matilde.fondo@usc.es

Author Contributions

The manuscript was written through contributions of all authors. All authors have given approval to the final version of the manuscript.

ACKNOWLEDGEMENTS

Authors thank the Spanish Ministerio de Innovación, Ciencia y Universidades (PGC2018-102052-B-C21, PGC2018-093863-B-C21 and MDM-2017-0767) for financial support. J.C.V thanks Xunta de Galicia for his Ph.D. fellowship. E.R. thanks Generalitat de Catalunya for an ICREA Academia award and for the SGR2017-1289 grant, and S.G.C. for a Beatriu de Pinòs grant. The authors acknowledge computer resources, technical expertise and assistance provided by the CSUC.

REFERENCES

(1) (a) Sessoli, R.; Gatteschi, D.; Caneschi, A., Novak, M. A. Magnetic bistability in a metal-ion cluster. *Nature* **1993**, *365*, 141-143; (b) Sessoli, R.; Tsai, H.-L.; Schake, A. R.; Wang, S.; Vincent, J. B.; Folting, K.; Gatteschi, D.; Christou, G.; Hendrickson, D. N. High-spin molecules: $[Mn_{12}O_{12}(O_2CR)_{16}(H_2O)_4]$. *J. Am. Chem. Soc*. **1993**, *115*, 1804-1816.

(2) Woodruff, D. N.; Winpenny, R. E. P.; Layfield, R. A. Lanthanide single-molecule magnets. *Chem. Rev*. **2013**, *113*, 5110−5148.

(3) Shiddiq, M.; Komijani, D.; Duan, Y.; Gaita-Ariño, A.; Coronado, E.; Hill, S. Enhancing coherence in molecular spin qubits via atomic clock transitions. *Nature* **2016**, *531*, 348–351.

(4) Lu, J.; Guo, M.; Tang, J. Recent developments in lanthanide single-molecule magnets. *Chem. Asian J*. **2017**, *12*, 2772–2779.

(5) Ishikawa, N.; Sugita, M.; Ishikawa, T.; Koshihara, S.; Kaizu, Y. Lanthanide double-decker complexes functioning as magnets at the single-molecular level. *J. Am. Chem. Soc.* **2003**, *125*, 8694–8695.

(6) Rinehart, J. D.; Long, J. R. Exploiting single-ion anisotropy in the design of f-element single-molecule magnets. *Chem. Sci.* **2011**, *2*, 2078–2085.

(7) Rinehart, J. D.; Fang, M.; Evans, W. J.; Long, J. R. A N_2^{3-} radical-bridged terbium complex exhibiting magnetic hysteresis at 14 K. *J. Am. Chem. Soc.* **2011**, *133*, 14236-1239.

(8) Chen, Y-C.; Liu, J-L.; Ungur, L.; Liu, J.; Li, Q-W.; Wang, L-F.; Ni, Z-P.; Chibotaru, L. F.; Chen, X-M.; Tong, M-L. Symmetry-supported magnetic blocking at 20 K in pentagonal bipyramidal Dy(III) single-ion magnets, *J. Am. Chem. Soc*. **2016**, *138*, 2829-2837.

(9) Ding, Y.-S.; Chilton, N. F.; Winpenny, R. E. P.; Zheng, Y.-Z. On approaching the limit of molecular magnetic anisotropy: a near-perfect pentagonal bipyramidal dysprosium(III) single-molecule magnet. *Angew. Chem., Int. Ed*. **2016**, *55*, 16071-16074.

(10) a) Guo, F.-S.; Day, B. M.; Chen, Y.-C.; Tong, M.-L.; Mansikkam-ki, A.: Layfield, R. A. A dysprosium metallocene single-molecule magnet functioning at the axial limit. *Angew. Chem. Int. Ed*. **2017**, *56*, 11445–11449. (b) Goodwin, C. A. P.; Ortu, F.; Reta, D.; Chilton, N. F.; Mills, D. P. Molecular magnetic hysteresis at 60 kelvin in dysprosocenium. *Nature* **2017**, *548*, 439–442.

(11) McClain, K. R.; Gould, C. A.; Chakarawet, K.; Teat, S. J.; Groshens, T. J.; Long, J. R.; Harvey, B. G. High-temperature magnetic blocking and magneto-structural correlations in a series of dysprosium(III) metallocenium single-molecule magnets *Chem. Sci*. **2018**, *9*, 8492-8503.

(12) Guo, F-S.; Day, B. M.; Chen, Y-C.; Tong, M-L.; Mansikkam-ki, A.; Layfield, R. A. Magnetic hysteresis up to 80 kelvin in a dysprosium metallocene single-molecule magnet. *Science* **2018**, *362*, 1400-1403.

(13) Gavey, E. L.; Beldjoudi, Y.; Rawson, J. M.; Stamatatos, T. C.; Pilkington, M. Slow relaxation in the first penta-aza Dy(III) macrocyclic complex. *Chem. Commun*. **2014**, *50*, 3741-3743.

(14) Mondal, A. K.; Goswami, S.; Konar, S. Influence of the coordination environment on slow magnetic relaxation and photoluminescence behavior in two mononuclear dysprosium(III) based single molecule magnets. *Dalton Trans*. **2015**, *44*, 5086-5094.

(15) Bar, A. K.; Kalita, P.; Sutter, J-P.; Chandrasekhar, V. Pentagonal-bipyramid Ln(III) complexes exhibiting Single-Ion-Magnet behavior: a rational synthetic approach for a rigid equatorial plane. *Inorg. Chem.* **2018**, *57*, 2398−2401.

(16) Fondo, M.; Corredoira-Vázquez, J.; García-Deibe, A. M.; Sanmartín-Matalobos, J.; Herrera, J. M.; Colacio, E. Tb_2, Dy_2 and Zn_2Dy_4 complexes showing the unusual versatility of a hydrazone ligand towards lanthanide ions: a magnetic study. *Inorg. Chem.* **2018**, *57*, 10100–10110.

(17) (a) Tamboura, F. B.; Diop, M.; Gaye, M.; Sall, A. S.; Barry, A. H.; Jouini, T. X-ray structure and spectroscopic properties of some lanthanides(III) complexes derived from 2,6-diacetylpyridine-bis(benzoylhydrazone). *Inorg. Chem. Commun*. **2003**, *6*, 1004–1010; (b) Tamboura, F. B.; Haba, P. M.; Gaye, M.; Sall, A. S.; Barry, A. H.; Jouini, T. *Polyhedron* **2004**, *23*, 1191–1197.

(18) Xue, S.; Zhao, L.; Guo, Y-N.; Deng, R.; Guo, Y.; Tang, J. A series of tetranuclear lanthanide complexes comprising two edge-sharing triangular units with field-induced slow magnetic relaxation for Dy_4 species. *Dalton Trans.* **2011**, *40*, 8347–8352.

(19) de Oliveira, G. M.; Machado, A.; Gomes, G. W. ; Monteiro, J. H. S. K.; Davolos, M. R.; Abram, U.; Jagst, A. Integrated X-ray crystallography, optical and computational methods in studies of structure and luminescence of new synthesized complexes of lanthanides with ligands derived from 2,6-diformylpyridine. *Polyhedron* **2011**, *30*, 851-859.

(20) Gao, X-S.; Wang, J-T. Two complexes of Eu^{3+} ion with pentadentate Schiff-base ligands exhibiting red photoluminescence. *Inorg. Chim. Acta* **2012**, *386*, 1–7.

(21) Kozłowski, M.; Kierzek, R.; Kubicki, M.; Radecka-Paryzek, W. *J.* Metal-promoted synthesis, characterization, crystal structure and RNA cleavage ability of 2,6-diacetylpyridine bis(2-aminobenzoylhydrazone) lanthanide complexes. *Inorg. Biochem*. **2013**, *126*, 38–45.

(22) Batchelor, L. J.; Cimatti, I.; Guillot, R.; Tuna, F.; Wernsdorfer, W.; Ungur, L.; Chibotaru, L. F.; Campbella, V. E.; Mallah, T. Chemical tuning of the magnetic relaxation in dysprosium(III) mononuclear complexes. *Dalton Trans*. **2014**, *43*, 12146–12149.

(23) Jiang, Z-X.; Liu, J-L.; Chen, Y-C.; Liu, J.; Jia, J-H.; Tong, M-L. Lanthanoid single-ion magnets with the LnN_{10} coordination geometry. *Chem. Commun*. **2016**, *52*, 6261—6264.

(24) González, A.; Gómez, E.; Cortés-Lozada, A.; Hernández, S.; Ramírez-Apan, T.; Nieto-Camacho, A. Heptacoordinate tin(IV) compounds derived from pyridine Schiff bases: synthesis, characterization, in vitro cytotoxicity, anti-inflammatory and antioxidant activity. *Chem. Pharm. Bull*. **2009**, *57*, 5—15.

(25) *SADABS: Area-Detector Absorption Correction*. Siemens Industrial Automation, Inc.: Madison, WI, 1996.

(26) Sheldrick, G. M. A short history of SHELX. *Acta Crystallogr., Sect. A: Found. Crystallogr*. **2008**, *A64*, 112−122.

(27) Malmqvist, P. Å.; Roos, B. O.; Schimmelpfennig, B., The restricted active space (RAS) state interaction approach with spin-orbit coupling. *Chem. Phys. Lett*. **2002**, *357*, 230-240.

(28) Roos, B. O.; Lindh, R.; Malmqvist, P.-A.; Veryazov, V.; Widmark, P.-O.; Borin, A. C., New relativistic atomic natural orbital basis sets for lanthanide atoms with applications to the Ce diatom and LuF_3. *J. Phys. Chem*. A **2008**, *112*, 11431-11435.

(29) Roos, B. O.; Lindh, R.; Malmqvist, P. Å.; Veryazov, V.; Widmark, P. O., Main group atoms and dimers studied with a new relativistic ANO basis set. *J. Phys. Chem. A* **2004**, *108*, 2851-2858.

(30) Widmark, P.-O.; Malmqvist, P.-k.; Roos, B. r. O., Density matrix averaged atomic natural orbital (ANO) basis sets for correlated molecular wave functions. *Theor. Chim. Acta* **1990**, *77*, 291-306.

(31) Fdez. Galván, I.; Vacher, M.; Alavi, A.; Angeli, C.; Aquilante, F.; Autschbach, J.; Bao, J. J.; Bokarev, S. I.; Bogdanov, N. A.; Carlson, R. K.; Chibotaru, L. F.; Creutzberg, J.; Dattani, N.; Delcey, M. G.; Dong, S. S.; Dreuw, A.; Freitag, L.; Frutos, L. M.; Gagliardi, L.; Gendron, F.; Giussani, A.; González, L.; Grell, G.; Guo, M.; Hoyer, C. E.; Johansson, M.; Keller, S.; Knecht, S.; Kovačević, G.; Källman, E.; Li Manni, G.; Lundberg, M.; Ma, Y.; Mai, S.; Malhado, J. P.; Malmqvist, P. Å.; Marquetand, P.; Mewes, S. A.; Norell, J.; Olivucci, M.; Oppel, M.; Phung, Q. M.; Pierloot, K.; Plasser, F.; Reiher, M.; Sand, A. M.; Schapiro, I.; Sharma, P.; Stein, C. J.; Sørensen, L. K.; Truhlar, D. G.; Ugandi, M.; Ungur, L.; Valentini, A.; Vancoillie, S.; Veryazov, V.; Weser, O.; Wesołowski, T. A.; Widmark, P.-O.; Wouters, S.; Zech, A.; Zobel, J. P.; Lindh, R., OpenMolcas: From source code to insight. *J. Chem. Theor. Comput.* **2019,** *15*, 5925-5964.

(32) Ungur, L.; Chibotaru, L. Strategies toward high-temperature lanthanide-based single-molecule magnets. *Inorg. Chem.* **2016**, *556*, 10043-10056.

(33) Drahonovsky, D.; Lehn, J-M. Hemiacetals in dynamic covalent chemistry. *J. Org. Chem*. **2009**, *74*, 8428–8432.

(34) Guidote, A. M. Jr.; Ando, K.; Kurusu, Y.; Nagao, H.; Masuyama, Y.; Syntheses and characterization of homodinuclear manganese and cobalt complexes bridged by a hemiacetal or by an acetato group in a μ–(η^2:η^1) bridging mode. *Inorg. Chim. Acta* **2001**, *314*, 27–36.

(35) Erxleben, A. Copper coordination to the aldehyde and hemiacetal form of 4-bromo-2-[(2-diethylaminoethyl)ethylaminomethyl]-6-formylphenol: Synthesis and structure of $[Cu(H_2L)_2(X)_2]X_2\ nH_2O$ (X = NO_3^-, ClO_4^-;) and $[Cu(L')]_2 \cdot 2CH_3OH$. *Inorg. Chim. Acta* **2009**, *362*, 839–844.

(36) Małecki, J. G.; Zwolinski, P. Synthesis, characterization and molecular structure of Pd(II) complex containing the methyl-hemiacetal form of isonicotinaldehyde. *Polyhedron* **2012**, *39*, 85–90.

(37) Barandov, A.; Abram, U. The formation of hemiacetal complexes of rhenium(V) by degradation of a Schiff base. *Z. Anorg. Allg. Chem*. **2013**, *639*, 2542–2547.

(38) Melekhova, A. A.; Novikov, A. S.; Rostovskii, N. V.; Sakharov, P. A.; Panikorovskii, T. L.; Bokach, N. A. Open-chain hemiketal is stabilized by coordination to a copper(II). *Inorg. Chem. Commun*. **2017**, *79*, 82-85.

(39) Mondal, D; Bhattacharya, K. Synthesis and structural characterization of a hemiacetal and aldehyde bound diiron(III) complex with two different coordination numbers: A product by oxidative cleavage of carbon-nitrogen single bond. *Inorg. Chem. Commun*. **2017**, *84*, 109-112.

(40) Nakamoto, K. *Infrared and Raman Spectra of Inorganic and Coordination Compounds*, Ed. John Wiley & Sons, New York, 1997.

(41) (a) Llunell, M.; Casanova, D.; Cirera, J.; Bofill, J. M.; Alemany, P.; Alvarez, S.; Pinsky, M.; Avnir, D. D. SHAPE v1.1b, Barcelona, **2005**. (b) Ruiz-Martínez, A.; Casanova, D.; Alvarez, S. Polyhedral structures with an odd number of vertices: nine-coordinate metal compounds. *Chem. Eur. J*. **2008**, *14*, 1291–1303. (c) Llunell, M.; Casanova, D.; Cirera, J.; Alemany, P.; Alvarez, S. SHAPE: Program for the stereochemical

analysis of molecular fragments by means of continuous shape measures and associated tools; University of Barcelona, Barcelona, Spain, **2010**.

(42) Allen, F. H. The Cambridge Structural Database: a quarter of a million crystal structures and rising. *Acta Crystallogr.* **2002**, *B58*, 380-388.

(43) Liles, D. C.; McPartlin, M.; Tasker, P. A.; Lip, H. C.; Lindoy, L. F. Novel polynuclear cadmium complexes resulting from ring-opening reactions of 2,6-bis(2-R-2-benzoxazolinyl)pyridine (R = Me or H); X-ray structures of $[Cd_4(C_{21}H_{17}N_3O_2)_2(MeCO_2)_4]\cdot Me_2NCHO\cdot H_2O$ and $[Cd_3(C_{19}H_{13}N_3O_2)_2(MeCO_2)_2(Me_2NCHO)_2]$. *J. Chem. Soc., Chem. Commun*. **1976**, 549-551.

(44) Potgieter, K.; Mayer, P.; Gerber, T. I. A.; Booysen, I. N. Coordination behavior of the multidentate Schiff base 2,6-bis(2-hydroxyphenyliminomethyl)pyridine towards the *fac*-$[Re(CO)_3]^+$ and $[ReO]^{3+}$ cores. *Polyhedron* **2009**, *28*, 2808–2812.

(45) Habarurema, G.; Gerber, T. I. A.; Hosten, E. C.; Betz, R. *Z.* Crystal structure of tricarbonyl-chlorido-(2*E*)-2-(6-(*E*-(2-hydroxyphenylimino)methyl)pyridine-2-yl)methyleneaminophenol-rhenium(I), $C_{22}H_{15}ClN_3O_5Re$. *Kristallogr. NCS* **2015**, *230*, 159-161

(46) Kose, M.; Goring, P. Lucas and V. Mckee, Mono-, di- and tri-nuclear manganese(II) complexes derived from a quinquedentate ligand: Superoxide dismutase and catalase mimetic studies. *Inorg. Chim. Acta* **2015**, *435*, 232–238.

(47) Janssen, F. F. B. J.; Peters, L. C. J. M.; Schlebos, P. P. J.; Smits, J. M. M.; de Gelder, R.; Rowan, A. E. Uncorrelated dynamical processes in tetranuclear carboxylate clusters studied by variable-temperature ^{1}H NMR spectroscopy *Inorg. Chem*. **2013**, *52*, 13004−13013.

(48) Sun, X-X.; Qi, C-M.; Ma, S-L.; Huang, H-B.; Zhu, W-X.; Liu, Y-C. Syntheses and structures of two Zn(II) complexes with the pentadentate Schiff-base ligands. *Inorg. Chem. Commun*. **2006**, *9*, 911–914.

(49) Kose, M. Two seven-coordinate Mn(II) complexes derived from pentadentate ligands: structural characterization and investigation of photophysical properties. *Inorg. and Nano-Metal Chem*. **2017**, *47*, 1711-1717.

(50) Kampert, E.; Janssen, F. F. B. J.; Boukhvalov, D. W.; Russcher, J. C.; Smits, J. M. M.; de Gelder, R.; de Bruin, B.; Christianen, P. C. M.; Zeitler, U.; Katsnelson, M. I.; Maan, J. C.; Rowan, A. E. Ligand-controlled magnetic interactions in Mn_4 clusters. *Inorg. Chem.* **2009**, *48*, 11903–11908.

(51) Lin, S-Y.; Wernsdorfer, W.; Ungur, L.; Powell, A. K.; Guo, Y-N.; Tang, J.; Zhao, L.; Chibotaru, L. F.; Zhang, H-J. Coupling Dy_3 triangles to maximize the toroidal moment. *Angew. Chem. Int. Ed.* **2012**, *51*, 12767–12771.

(52) (a) Fondo, M.; Corredoira-Vázquez, J.; García-Deibe, A. M.; Sanmartín-Matalobos, J.; Herrera, J. M.; Colacio, E. Designing ligands to isolate ZnLn and Zn_2Ln complexes: field-induced single-ion magnet behavior of the ZnDy, Zn_2Dy, and Zn_2Er analogues. *Inorg. Chem*. **2017**, *56*, 5646-5656. (b) Fondo, M.; Corredoira-Vázquez, J.; Herrera-Lanzós, A.; García-Deibe, A. M.; Sanmartín-Matalobos, J.; Herrera, J. M.; Colacio, E.; Nuñez, C. Improving the SMM and luminescence properties of lanthanide complexes with LnO_9 cores in the presence of ZnII: an emissive Zn_2Dy single ion magnet. *Dalton Trans*. **2017**, *46*, 17000–17009.

(53) Das, C.; Upadhyay, A.; Shanmugam, M. Influence of radicals on magnetization relaxation dynamics of pseudo-octahedral lanthanide iminopyridyl complexes. *Inorg. Chem*. **2018**, *57*, 9002−9011.

(54) Yu, S.; Hu, Z.; Chen, Z.; Li, B.; Zhang, Y-Q.; Liang, Y.; Liu, D.; Yao, D.; Liang, F. Two Dy(III) single-molecule magnets with their performance tuned by Schiff Base ligands. *Inorg. Chem*. **2019**, *58*, 1191−1200.

(55) (a) Friedman, J. R.; Sarachick, M. P.; Tejada, J.; Ziolo, R. Macroscopic measurement of resonant magnetization tunneling in high-spin molecules. *Phys. Rev. Lett*. **1996**, *76*, 3830–3833; (b) Thomas, L.; Lionti, F.; Ballou, R.; Gatteschi, D.; Sessoli, R.; Barbara, B. Macroscopic quantum tunnelling of magnetization in a single crystal of nanomagnets. *Nature* **1996**, *383*, 145–147.

(56) Ruiz, J.; Mota, A. J.; Rodríguez-Diéguez, A.; Titos, S.; Herrera, J. M.; Ruiz, E.; Cremades, E.; Costes, J. P.; Colacio, E. Field and dilution effects on the slow relaxation of a luminescent DyO_9 low-symmetry single-ion magnet. *Chem. Commun*. **2012**, *48*, 7916-7918.

(57) Day, B. M.; Guo, F-S., Layfield, R. A. Cyclopentadienyl ligands in lanthanide single-molecule magnets: one ring to rule them all? *Acc. Chem. Res*. **2018**, *51*, 1880−1889, and references therein.

(58) Chilton, N. F.; Collison, D.; McInnes, E. J. L.; Winpenny, R. E. P.; Soncini, A. An electrostatic model for the determination of magnetic anisotropy in dysprosium complexes. *Nat. Commun.* **2013**, *4*, 2551.

(59) Aravena, D.; Ruiz, E. Shedding light on the single-molecule magnet behavior of mononuclear Dy^{III} complexes. *Inorg. Chem.* **2013**, *52*, 13770-13778.

(60) Gomez-Coca, S.; Aravena, D.; Morales, R.; Ruiz, E. Large magnetic anisotropy in mononuclear metal complexes. *Coord. Chem. Rev.* **2015,** *289*, 379-392.

(61) Atanasov, M.; Aravena, D.; Suturina, E.; Bill, E.; Maganas, D.; Neese, F. First principles approach to the electronic structure, magnetic anisotropy and spin relaxation in mononuclear 3d-transition metal single molecule magnets. *Coord. Chem. Rev.* **2015,** *289*, 177-214.

(62) Malrieu, J. P.; Caballol, R.; Calzado, C. J.; de Graaf, C.; Guihéry, N. Magnetic interactions in molecules and highly correlated materials: physical content, analytical derivation, and rigorous extraction of magnetic hamiltonians. *Chem. Rev.* **2014,** *114*, 429-492.

(63) Aravena, D. Ab initio prediction of tunneling relaxation times and effective demagnetication barriers in Kramers lanthanide single-molecule magnets. *J. Phys. Chem. Lett.* **2018**, *9*, 5327-5333.

Table of Contents Graphic and Synopsis

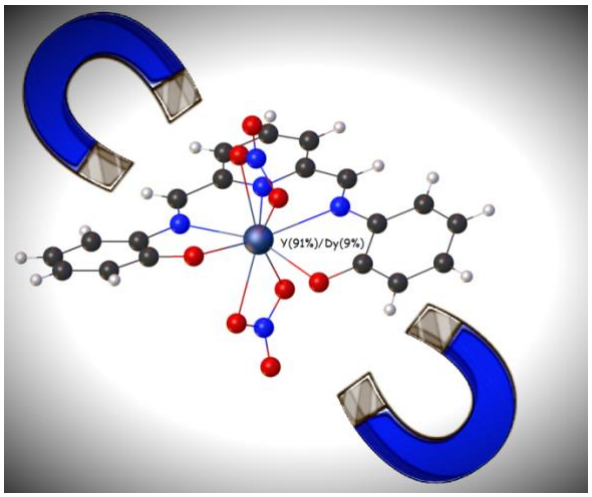

Hitherto unknown lanthanoid complexes of a related flat N_3O_2 donor show *ac* susceptibility frequency-dependence, $(Et_3NH)[Dy_{0.09}Y_{0.91}(L)(NO_3)_2]$ being a SIM at zero field.